Laser absorption and third-harmonic generation in free-electron nanofilms

Sergey V. Fomichev,[1,2,*] David F. Zaretsky,[1,2,†] and Wilhelm Becker[2,‡]
[1]*Russian Research Center "Kurchatov Institute," Institute of Molecular Physics, Kurchatov Place 1, 123182 Moscow, Russia*
[2]*Max-Born-Institut für Nichtlineare Optik und Kurzzeitspectroskopie, Max-Born-Straße 2A, 12489 Berlin, Germany*
(Received 28 July 2008; revised manuscript received 2 January 2009; published 27 February 2009)

The collective collisionless dynamics of the electron gas in free-electron nanofilms irradiated by an obliquely incident *p*-polarized laser wave are considered in the classical hydrodynamic and jellium-model approximations. The two cases of cold metallic nanofilms and hot free-electron nanofilms laser ionized and laser heated by a pump-laser prepulse are investigated with proper electron statistics. Both linear and nonlinear properties of the plasma resonance excitation in the nanofilms are studied in detail for different film parameters (film thickness, thickness of the diffuse film boundary, outer-ionization degree for hot laser-ionized/heated films, etc.). The significant role of the diffuse film boundaries for both linear absorption of the laser field and third-harmonic generation is demonstrated. For this goal, we do not use the standard dielectric-permittivity approach with boundary conditions between two different media but solve continuously over all space the full set of hydrodynamic and electrodynamic equations in nonrelativistic one-dimensional approximation. It is shown that collisionless edge absorption may be dominant in thin nanofilms, while in cold metal nanofilms it results in the appearance of several linear-absorption resonances below the bulk-plasma resonance frequency. For hot nanofilms, drastic broadening of the linear-plasma-resonance profile is obtained in calculations when the film thickness is reduced. In our model, the third-harmonic generation is determined by the density gradient in the diffuse film edges. Additional resonances in third-harmonic generation as a function of laser frequency are obtained for cold metal nanofilms. They differ from the standard third-order nonlinear resonance, which is located at one third of the plasma resonance frequency. The important role of the outer-ionization degree in forming the third-order nonlinear response of the hot laser-ionized film is also analyzed and discussed.

DOI: 10.1103/PhysRevB.79.085431 PACS number(s): 52.38.Dx, 42.65.Ky, 73.22.Lp, 78.67.-n

I. INTRODUCTION

The interaction of a strong laser field with various nano-objects has been actively investigated over the last decades. It was established both theoretically and experimentally that the small dimensions of free-electron nano-objects (both metal and laser-ionized nanoclusters, nanorods, nanofilms, nanowires, etc.) are responsible for the appearance of new effects in the confined electron nanoplasma excited by the laser field. For example, in nanoclusters the collective oscillations of the electron cloud in the laser field are nonlinear. As a result, the generation of at least the third harmonic due to this collective electron motion is possible. This was experimentally observed both for cold (gold and silver) metal clusters[1–3] and for argon clusters that are laser ionized in the strong laser field.[4] The probability of third-harmonic generation in clusters is much enhanced if this harmonic is in resonance with the Mie frequency.[5–11] Another qualitative difference between small nanoclusters on one hand and large clusters and bulk on the other hand is that in the former, surface electron scattering may be the dominant damping mechanism,[12,13] at least in the linear regime for linear polarization. It was shown exactly by theoretical analysis[14] of the collisionless Vlasov equation that the mechanism of light absorption in cold metal nanoclusters is modified with respect to that in an unbounded plasma: laser absorption in nanoclusters with a steplike boundary of the ion core is mainly due to electron collisions with the cluster boundary, so the corresponding width of the Mie plasma resonance increases with decreasing cluster radius. This absorption mechanism can also be interpreted as the irreversible part of Landau damping in a finite plasma system. Different collisionless absorption mechanisms in both linear and nonlinear laser-cluster interactions for different laser polarizations were also considered recently.[15–19]

The effect of the nonlinearity of the electron oscillations under the action of a laser field should also be present in nanofilms (in metallic films or in any laser-heated/ionized films with free electrons). Owing to the small film thickness, the effect may be important for the light polarization perpendicular to the film surface. The small film thickness should also be important for the absorption mechanism that was demonstrated experimentally for cantilever (freely suspended) ultrathin carbon films irradiated by a strong laser field.[20] Theoretically, the linear and nonlinear absorptions of laser radiation in thin films with steplike boundaries were considered recently in Refs. 21–23 (the older references[24–26] should also be mentioned). Actually, the film boundary may be diffuse rather than steplike, and for a quantitative description this has to be taken into account. This should be especially important for the nonlinear oscillations of the electron cloud because it was shown that for clusters with steplike ion boundary, the nonlinear terms (e.g., the third-order nonlinearity) are proportional to the electron-density gradient at the cluster boundary.[6,27] Also, for clusters interacting with strong laser fields, a model that takes into account the spatial nonuniformity of the cluster as it evolves in time due to Coulomb explosion was recently developed,[28] and an enhancement of the laser absorption as compared with the uniform density model was obtained in the calculations.

The aim of this paper is to consider the dynamics of the collective electron motion in thin nanofilms in the presence of laser fields of moderate intensity, such that the nonrelativ-

istic approximation for the electron motion is still applicable. Both the linear and the nonlinear dynamics of the transverse electron motion in a p-polarized laser field are considered, taking into account the effects of diffuse boundaries of the thin film. Both linear light absorption and third-harmonic generation will be investigated in dependence of the laser and film parameters including the thickness of the film and the thickness of the diffuse film boundaries. Generally, a proper consideration of this problem should use the quantum microscopic self-consistent equations based on the Kohn-Sham density-functional theory. Such equations in the random-phase approximation (RPA) or in the time-dependent local-density approximation (TDLDA) can be successfully applied to the numerical description of the linear and nonlinear dynamics of small clusters with radii of the order of a few nanometers[29,30] but no more because even now with modern computational capabilities, it is very hard to apply them to larger nano-objects. Alternatively, in order to examine the excitation properties of the transverse plasma resonance in a thin metallic nanofilm, the numerical solution of the kinetic (Vlasov) equations for the electron-ion subsystem together with the Maxwell equations for the electromagnetic field inside and outside the film can be employed. For cold metal nanofilms, such an approach was used recently.[31–33] However, much information about these processes may be obtained already with the somewhat simpler hydrodynamic equations.

In this paper, we use the hydrodynamic approach for describing the collective electron motion and the properties of the transverse plasma resonance in thin free-electron nanofilms under the action of a p-polarized laser field. We restrict ourselves to slab geometries such that a one-dimensional approximation can be safely used. Because we consider films with diffuse boundaries, we do not make use of the concept of the dielectric permittivity. Rather, we solve the full set of the respective hydrodynamic and electrodynamic equations for the electrons moving in the laser field, taking into exact account the effects of spatial dispersion of the electron gas in a finite system. Even though the final results were obtained numerically, a lot of analytical work was performed before [in contrast to purely numerical particle-in-cell (PIC) simulations, which have become very popular] in order to reduce the full set of the corresponding partial differential equations (PDEs) to a few ordinary ones or even to algebraic expressions and to facilitate the numerical calculations in this very stiff PDE problem.

Note that the hydrodynamic approach developed in this paper for thin nanofilms is classical, except for the Fermi statistics used in the case of a cold metallic nanofilm. This approach can be regarded as an adaptation to films of similar classical hydrodynamic models used earlier for the description of second-harmonic generation from metal surfaces.[34–37] Quantum effects such as quantization of the transverse electron motion are not taken into account in this approach. It does not allow us only to consider extremely thin films. For cold metal films, the criterion for the minimum film thickness a can simply be taken from the uncertainty relation as $\hbar/a \ll p_F$, where p_F is the Fermi momentum of the electrons. With typical values[38] of $p_F/\hbar \sim 10$ nm^{-1}, classical hydrodynamics appear to be applicable for nanofilms with thickness in the range of $1 \ll a \lesssim 100$ nm, which are those that we shall consider. For hot laser-heated nanofilms with classical Boltzmann statistics the corresponding criterion is well satisfied. In contrast, the quantum effects associated with the degeneracy of the electron gas in cold metal nanofilms are included. More importantly, the jellium-model approximation used in this paper for the ion-density distribution may be justified only for simple metals with a closed and simply connected Fermi surface (at least in the case of weak external electron excitations for cold metallic nanofilms).

This paper is organized as follows. Section II contains the statement of the problem of the laser-film interaction in the hydrodynamic approximation. The hydrodynamic model employed and the basic equations are described in Sec. II A. An outline of the corresponding static problem is presented in Sec. II B both for cold metal films (Sec. II B 1) and for hot laser-heated/ionized films (Sec. II B 2). Results for the dynamical problem, both linear and nonlinear, are presented in Secs. III and IV. Section III contains the results for the benchmark case of a neutral film with a zero value of the crucial (dimensionless) film parameter A defined in Eq. (6) in Sec. II A. (The main effect of nonzero A is a deviation of the static electron density from the ion-charge density near the film boundaries, while for $A=0$ in the static regime complete local compensation of the positive and negative charges takes place in all parts of the film.) For the specific case of $A=0$, the results of the linear approximation with respect to the laser field are presented in Sec. III A, and the second-order and the third-order nonlinear responses of the film are discussed in Sec. III B. In Sec. IV, we consider the general case of $A \neq 0$. Again, the results of the linear approximation with respect to the laser field are exhibited in Sec. IV A, while the third-order nonlinear response is investigated in Sec. IV B. In this case cold metal films are examined in Secs. IV A 1 and IV B 1, while hot laser-heated/ionized films are inspected in Secs. IV A 2 and IV B 2. Concluding remarks terminate the paper in Sec. V.

II. HYDRODYNAMIC APPROACH TO THE LASER-FILM INTERACTION

A. Basic equations

We consider the case when the electron velocity is small compared with the speed of light and neglect the magnetic part of the Lorentz force. The latter is especially safe for thin nanofilms under conditions when the transverse dipole approximation can be applied. We also assume that the ion subsystem is frozen on the femtosecond time scale, and we do not take into account electron-ion or electron-electron binary collisions. Under these conditions, the collisionless hydrodynamic equations for the time-dependent macroscopic spatial distributions of the electron density $n_e(t,\boldsymbol{r})$, the average electron velocity $\overline{\boldsymbol{v}}(t,\boldsymbol{r})$, and the electron pressure tensor $P_{\alpha\beta}(t,\boldsymbol{r})$ are

$$\frac{\partial n_e}{\partial t} + \mathrm{div}(n_e \overline{\boldsymbol{v}}) = 0,$$

$$n_e m_e \left(\frac{\partial \bar{v}_\alpha}{\partial t} + \bar{v}_\beta \frac{\partial \bar{v}_\alpha}{\partial x_\beta} \right) + \frac{\partial P_{\alpha\beta}}{\partial x_\beta} + e n_e (E_\alpha + E_{L\alpha}) = 0,$$

$$\frac{\partial P_{\alpha\beta}}{\partial t} + \bar{v}_\gamma \frac{\partial P_{\alpha\beta}}{\partial x_\gamma} + P_{\alpha\gamma} \frac{\partial \bar{v}_\beta}{\partial x_\gamma} + P_{\beta\gamma} \frac{\partial \bar{v}_\alpha}{\partial x_\gamma} + P_{\alpha\beta} \frac{\partial \bar{v}_\gamma}{\partial x_\gamma} = 0. \quad (1)$$

These equations describe the collective dynamics of the free-electron gas of a nano-object exposed to the laser field if the linear size of the nano-object in the field direction (of the order of 10–100 nm) is smaller than the electron mean-free path due to binary collisions. Here, m_e is the electron mass, e is the absolute value of the electron charge, $\boldsymbol{E}_L(t,\boldsymbol{r})$ is the electric field of the incident laser pulse, and $\boldsymbol{E}(t,\boldsymbol{r})$ is the self-consistent electric field of the ions and electrons. Equations (1) can be directly obtained from the collisionless Vlasov kinetic equation for the electron distribution function $f_e(t,\boldsymbol{r},\boldsymbol{p})$ (with $\boldsymbol{p}=m_e\boldsymbol{v}$),

$$\frac{\partial f_e}{\partial t} + v_\alpha \frac{\partial f_e}{\partial x_\alpha} - e(E_\alpha + E_{L\alpha}) \frac{\partial f_e}{\partial p_\alpha} = 0, \quad (2)$$

by integrating Eq. (2) over momentum, respectively, with factors 1, v_α, and $v_\alpha v_\beta$.[39,40] In this case, $n_e=\int f_e d^3p$, $\bar{\boldsymbol{v}}=n_e^{-1}\int \boldsymbol{v} f_e d^3p$, and $P_{\alpha\beta}=m_e\int (v_\alpha-\bar{v}_\alpha)(v_\beta-\bar{v}_\beta) f_e d^3p$.

The self-consistent electric field $\boldsymbol{E}(t,\boldsymbol{r})$ can be found from the Maxwell equation

$$\mathrm{div}\, \boldsymbol{E} = 4\pi e(z_i n_i - n_e), \quad (3)$$

where $n_i(\boldsymbol{r})$ is the spatial distribution of the density of the positive ions and z_i is the mean ionic charge. Equation (3) should be used already in the corresponding static (quasi-equilibrium) problem prior to the action of the laser pulse (prior to the action of the probe pulse in the case of laser-heated/ionized nano-objects). In the slab geometry that we consider, i.e., for nanofilms oriented perpendicularly to the z axis, the jellium-model ion density can be represented as $n_i(z)=n_{\mathrm{ion}}$ for $|z|-a/2\le -\sigma/2$, $n_i(z)=0$ for $|z|-a/2\ge \sigma/2$, and $n_i(z)=n_{\mathrm{ion}}g[(|z|-a/2)/\sigma]$ for $||z|-a/2|<\sigma/2$, where a is the film thickness and n_{ion} is the reference bulk ion density. The parameter σ characterizes the diffuseness of the film edge (we understand that the condition $\sigma \ll a$ is always satisfied) and the dimensionless function $g(x)$ specifies the profile of the film-boundary edge [with the dimensionless argument $x=(|z|-a/2)/\sigma$, where $|x|<1/2$].

If $\sigma=0$, then $n_i(z)=0$ for $|z|>a/2$ and $n_i(z)=n_{\mathrm{ion}}$ for $|z|\le a/2$ (the steplike ion density). For $\sigma\neq 0$, the simplest continuous trapezoidal profile $g(x)\equiv g_1(x)=-x+0.5$ can be used to model the ion background at the film edges. Alternatively, polynomial profiles can be used as shown in Fig. 1, which have smoother behavior at $x=\pm 1/2$: $g(x)\equiv g_2(x)=2x^3-1.5x+0.5$ (with continuous first derivative), $g(x)\equiv g_3(x)=-6x^5+5x^3-1.875x+0.5$ (with continuous second derivative), and $g(x)\equiv g_4(x)=20x^7-21x^5+8.75x^3-2.1875x+0.5$ (with continuous third derivative). We will generally assume that the film is symmetric with respect to its center $z=0$.

For thin nanofilms with thickness a much smaller than both the laser-spot diameter ($a\ll D$) and the laser wavelength ($a\ll\lambda$), we can consider the electron density and all other electron parameters as homogeneous in the directions along the film. For an obliquely incident linearly polarized laser pulse, the problem can be considered as one-dimensional, depending only on the z coordinate perpendicular to the film. The derivatives with respect to the longitudinal coordinates x and y can be dropped, and the full system of one-dimensional equations for the transverse collective electron motion in the slab under the action of the laser field can be written as

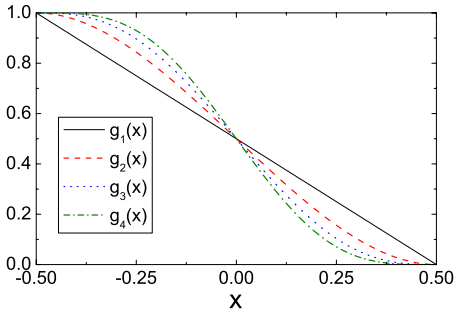

FIG. 1. (Color online) The model film edge profiles $g_i(x)$ of different smoothness ($i=1-4$, see text) with $x=(|z|-a/2)/\sigma$.

$$\frac{\partial n_e}{\partial t} + \frac{\partial (n_e \bar{v}_z)}{\partial z} = 0, \quad \frac{\partial E_z}{\partial z} - 4\pi e z_i n_i + 4\pi e n_e = 0,$$

$$m_e n_e \left(\frac{\partial \bar{v}_z}{\partial t} + \bar{v}_z \frac{\partial \bar{v}_z}{\partial z} \right) + \frac{\partial P_{zz}}{\partial z} + e n_e (E_{Lz} + E_z) = 0,$$

$$\frac{\partial P_{zz}}{\partial t} + \bar{v}_z \frac{\partial P_{zz}}{\partial z} + 3 P_{zz} \frac{\partial \bar{v}_z}{\partial z} = 0. \quad (4)$$

We will consider a p-polarized electromagnetic wave since only an electric-field component directed into the film will drive electrons so that they experience the finite thickness of the film and its boundary. For a wave of frequency ω propagating at an angle θ with respect to the z axis normal to the film, the z component of its electric field with the peak amplitude E_0 can be taken in the transverse dipole approximation as homogeneous,

$$E_{Lz}(t) = E_0 \sin\theta f_L(t/t_p)\cos(\omega t + \varphi),$$

where $f_L(t/t_p)$ is the envelope of the pulsed laser electric field normalized to unity at its maximum, t_p is the pulse duration, and φ is the carrier-envelope phase.

To rewrite Eqs. (4) in dimensionless form, let us introduce the dimensionless variables $\tau=\omega t$, $\zeta=z/a$, $n=n_e/(z_i n_{\mathrm{ion}})$, $u=\bar{v}_z/(\omega a)$, $f=E_z/(4\pi e z_i n_{\mathrm{ion}} a)$, and $\Theta_i(\zeta)=n_i(\zeta a)/n_{\mathrm{ion}}$ [$\Theta_i(\zeta)=1$ for $|\zeta|\le(1-\tilde{\sigma})/2$, $\Theta_i(\zeta)=0$ for $|\zeta|\ge(1+\tilde{\sigma})/2$, and $\Theta_i(\zeta)=g(x)$ for $|\zeta|=1/2+\tilde{\sigma}x$, with $|x|<1/2$ and with the dimensionless diffuseness $\tilde{\sigma}=\sigma/a$ at the film boundary]. Here, the normalization length is chosen as the overall film thickness a. Besides, we define the dimensionless electron current as $q=nu$ and the dimensionless electron pressure as $P=P_{zz}/P_0$, where P_0 is the reference electron pressure to be specified in Sec. II B, which corresponds to the quasiequilibrium electron distribution prior to the action of the probe-

laser pulse. With these notations, the system of equations for the time-dependent dimensionless functions $n(\tau,\zeta)$, $q(\tau,\zeta)$, $P(\tau,\zeta)$, and $f(\tau,\zeta)$ is

$$\frac{\partial n}{\partial \tau}+\frac{\partial q}{\partial \zeta}=0, \quad \frac{\partial f}{\partial \zeta}-\Theta_i(\zeta)+n=0, \tag{5a}$$

$$\frac{\partial q}{\partial \tau}+\frac{\omega_p}{\omega}\gamma q+\frac{\partial (q^2/n)}{\partial \zeta}+\frac{\omega_p^2}{\omega^2} \times\left\{A\frac{\partial P}{\partial \zeta}+nf_L(\tau/\tau_p)\frac{1}{2}(e_L e^{-i\tau}+e_L^{\star}e^{i\tau})+nf\right\}=0, \tag{5b}$$

$$\frac{\partial P}{\partial \tau}+\frac{q}{n}\frac{\partial P}{\partial \zeta}+3P\frac{\partial (q/n)}{\partial \zeta}=0. \tag{5c}$$

Here $\omega_p=\sqrt{4\pi e^2 z_i n_{\mathrm{ion}}/m_e}$ is the nominal (bulk) plasma frequency, $e_L=E_0 \sin\theta e^{-i\varphi}/(4\pi e z_i n_{\mathrm{ion}} a)$ is the dimensionless complex amplitude of the z component of the incoming laser electric field, $f_L(\tau/\tau_p)$ is the laser-pulse profile with dimensionless pulse duration $\tau_p=\omega t_p$, and

$$A=P_0/(4\pi e^2 z_i^2 n_{\mathrm{ion}}^2 a^2) \tag{6}$$

defines the dimensionless film parameter whose decisive role will already become clear in Sec. II B. The relaxation term with the dimensionless relaxation constant γ, which is normalized to the nominal plasma frequency ω_p, was introduced phenomenologically in Eq. (5b). We include this collisionlike term, which simulates weak binary collisions, because the solution of Eqs. (5a)–(5c) even in the collisionless case implies the limit of $\gamma\to+0$, which does not coincide with the result of direct substitution $\gamma=0$. Mathematically, the situation is the same as for the collisionless Landau damping problem[40] when introducing the *infinitesimal* collision term in the kinetic equation results in *finite* dissipation.

Equations (5a)–(5c) are nonlinear and can describe both the linear and the nonlinear transverse electromagnetic responses of the nanofilms. In our hydrodynamic model, nonlinearities are present in Eqs. (5b) and (5c). They come from the electric force density in Eq. (5b) and from the gradient term $\partial(q^2/n)/\partial\zeta$ in Eq. (5b) and two similar gradient terms in Eq. (5c). In the case of $A\neq 0$ and at moderate laser intensities (see details in Sec. IV), all these sources of nonlinearity may be of the same order and work together, resulting in the total physical nonlinearity due to the density gradient in the diffuse film boundaries. In the benchmark case of $A=0$ in Eq. (5b) (see Sec. III), Eq. (5c) is decoupled and only the nonlinearities of Eq. (5b) contribute to harmonic generation.

Equations (5a)–(5c) can be solved with the initial condition of a neutral cold electron plasma before the arrival of the laser pulse. This would allow one to study the plasma resonance properties in cold metal nanofilms, absorption of the laser pulse, and harmonic generation. Another problem is to study the properties of linear and nonlinear excitations of the transverse plasma resonance in the laser-heated film. This corresponds to a typical pump-probe experiment when a relatively weak probe pulse is used to obtain the response of the film, which is already excited by the strong pump pulse. In both cases, the initial conditions to the dynamic equations must be found from the corresponding static equations for the equilibrium distributions $n_s(\zeta)$ and $f_s(\zeta)$ of the electron density and the self-consistent electric field, respectively,

$$A\frac{dP_s}{d\zeta}+n_s f_s=0, \quad \frac{df_s}{d\zeta}=\Theta_i(\zeta)-n_s. \tag{7}$$

The equilibrium electron pressure P_s should be expressed through the equilibrium electron density n_s and the electron temperature.

B. Outline of the static problem

In equilibrium, the local electron pressure P_{zz} is a function of the local electron density n_e and the electron temperature. For the sake of generality, we consider the case of quasiequilibrium with different longitudinal and transverse electron temperatures $T_\parallel$ and $T_\perp$ (with respect to the z direction normal to the film), which can be relevant at least for laser-heated hot nanofilms. By generalizing the common Fermi distribution[41] for electrons to this case, the electron density and pressure are related by the implicit expressions

$$n_e=\frac{2}{(2\pi\hbar)^3}\int_{-\infty}^{+\infty}\frac{dp_x dp_y dp_z}{\exp\left(\frac{p_x^2+p_y^2}{2m_e T_\perp}+\frac{p_z^2}{2m_e T_\parallel}-\varkappa\right)+1} =\frac{(2m_e)^{3/2}T_\perp T_\parallel^{1/2}}{\pi^2\hbar^3}\int_0^{+\infty}\frac{p^2dp}{e^{p^2-\varkappa}+1}, \tag{8a}$$

$$P_{zz}=\frac{2m_e}{(2\pi\hbar)^3}\int_{-\infty}^{+\infty}\frac{v_z^2 dp_x dp_y dp_z}{\exp\left(\frac{p_x^2+p_y^2}{2m_e T_\perp}+\frac{p_z^2}{2m_e T_\parallel}-\varkappa\right)+1} =\frac{(2m_e)^{5/2}T_\perp T_\parallel^{3/2}}{3m_e\pi^2\hbar^3}\int_0^{+\infty}\frac{p^4dp}{e^{p^2-\varkappa}+1}, \tag{8b}$$

where $\varkappa$ is a normalization parameter. In the current quasiequilibrium case with different longitudinal and transverse temperatures, it replaces the ratio of the chemical potential to the common temperature $T=T_\perp=T_\parallel$ in the case of full thermal equilibrium. As a result,

$$P_{zz}=n_e T_\parallel F\left(\frac{\varepsilon_F^{3/2}}{3T_\perp T_\parallel^{1/2}}\right), \tag{9}$$

where $\varepsilon_F=(3\pi^2)^{2/3}\hbar^2 n_e^{2/3}/(2m_e)$ is the local Fermi energy and the function $F(x)$ is defined by the equations

$$F(x)=\frac{2}{3x}\int_0^{+\infty}\frac{p^4dp}{e^{p^2-\varkappa}+1}, \quad \int_0^{+\infty}\frac{p^2dp}{e^{p^2-\varkappa}+1}=x. \tag{10}$$

For $x\ll 1$ (in the limit of high temperatures) $F(x)\approx 1$ and $P_{zz}=n_e T_\parallel$. In the opposite limiting case of $x\gg 1$ (for cold metal nanofilms) $F(x)\approx\frac{2}{5}(3x)^{2/3}$ and $P_{zz}=\frac{2}{5}n_e\varepsilon_F(T_\parallel/T_\perp)^{2/3}$.

1. Cold metal films

For cold metal nanofilms at the initial equilibrium temperature $T_\parallel=T_\perp=T_0\ll\varepsilon_F^{(0)}$, where the reference (bulk) Fermi energy is $\varepsilon_F^{(0)}=(3\pi^2)^{2/3}\hbar^2(z_i n_{\mathrm{ion}})^{2/3}/(2m_e)$, we can set the ref-

erence electron pressure to $P_0=\frac{2}{5}z_i n_{\rm ion}\varepsilon_F^{(0)}$. Hence, $P_s=n_s^{5/3}$ and the film parameter A defined by Eq. (6) may be expressed through the squared ratio of two lengths as $A=(l_Q/a)^2$, with $l_Q=3^{1/3}\pi^{1/6}\hbar/[e\sqrt{20m_e(z_i n_{\rm ion})^{1/6}}]$. The quantum length l_Q is of the order of $\sqrt{\varepsilon_F^{(0)}}/(4\pi e^2 z_i n_{\rm ion})$, which corresponds to the expression for the classical Debye length,[41] with the temperature substituted by $\varepsilon_F^{(0)}$. The parameter A decreases with increasing film length a. Typical values of the length l_Q, which can be interpreted as a "quantum Debye screening length," are in the range of a few hundredth of a nanometer [from 0.036 nm for Be with[38] $z_i n_{\rm ion}=24.2\times10^{22}$ cm^{-3} up to 0.062 nm for Cs with[38] $z_i n_{\rm ion}=0.91\times10^{22}$ cm^{-3}]. Hence, typical values of the dimensionless parameter A for cold metal nanofilms with thickness $a=100$ nm are of the order of 10^{-7}. Even for films with thickness $a=10$ nm, the parameter A is of the order of 10^{-5}. Because on the average the interatomic distance in metals can be estimated[38] by 0.3 nm (and this length can be considered as the minimal edge diffuseness), it seems that even the diffuseness of the film edges, not to mention the film thickness, is always much larger than the quantum length l_Q, i.e., $\sigma \gg l_Q$.

For $A=0$, the solution of the static Eq. (7) is $f_s(\zeta)=0$ and $n_s(\zeta)=\Theta_i(\zeta)$. This means that in this limiting case the negative electron-charge density totally compensates the positive ion-charge density. In other words, the screening of the positive charges by the negative ones is locally complete over the whole film. This can be interpreted as the consequence of a vanishing quantum Debye screening length l_Q in this approximation. So, the case of $A=0$ can be regarded as a zeroth-order approximation for cold globally uncharged metal films with diffuse edges.

To first order with respect to A, the solution of Eq. (7) with $P_s=n_s^{5/3}$ can be analytically obtained as

$$f_s=-\frac{5A}{2}\frac{d\Theta_i^{2/3}}{d\zeta},\quad n_s=\Theta_i+\frac{5A}{2}\frac{d^2\Theta_i^{2/3}}{d\zeta^2}. \tag{11}$$

It is clear that this solution can be applicable only under the condition of $A\ll\tilde{\sigma}^2$ (which is equivalent to $l_Q\ll\sigma$). Equation (7) for cold metal nanofilms can be numerically solved as a boundary-value problem with boundary conditions $f_s[\mp(1+\tilde{\sigma})/2]=0$, which corresponds to a cold neutral film (with zero total charge). In this case, it is assumed that outside the film [for $|\zeta|>(1+\tilde{\sigma})/2$] both $n_s(\zeta)=0$ and $f_s(\zeta)=0$. This means that we do not take into account the purely quantum effect of electron spill out, which is defined by the metal work function. For numerical solution of Eq. (7), it is convenient to introduce the new variables $\tilde{\zeta}=\zeta/\sqrt{A}$ and $\tilde{f}_s=f_s/\sqrt{A}$; for cold metal nanofilms Eq. (7) is then rewritten as

$$\frac{5}{3}\frac{dn_s}{d\tilde{\zeta}}+n_s^{1/3}\tilde{f}_s=0,\quad \frac{d\tilde{f}_s}{d\tilde{\zeta}}=\Theta_i(\tilde{\zeta}\sqrt{A})-n_s. \tag{12}$$

This means that the normalization length in the dimensionless variables is now the "quantum Debye length" l_Q rather than the film thickness a. The exact solutions of Eq. (12) for $n_s(\zeta)$ and $\tilde{f}_s(\zeta)$ are presented in Fig. 2 for the typical case of $A=10^{-6}$. The electron density has a steplike behavior near the film boundary, and the discontinuity decreases as the boundary diffuseness increases. We observe that nonzero A is responsible for creating a nonuniformly charged double layer on the surface of the metal film. The corresponding electric field keeps the electrons inside the cold metal film. Near its boundary the maximal value of this field is $E_z^{\max}\approx0.4\times4\pi e z_i n_{\rm ion} l_Q$ for $\tilde{\sigma}=10^{-3}-10^{-2}$, and it is of the order of 10^8 V/cm! Therefore, an incident electromagnetic field that is weaker than this value (that is, its intensity is below 10^{13} W/cm^2) can be regarded as a perturbation (in the regime of weak nonlinearity) from the point of view of the collective electron dynamics in metal nanofilms.

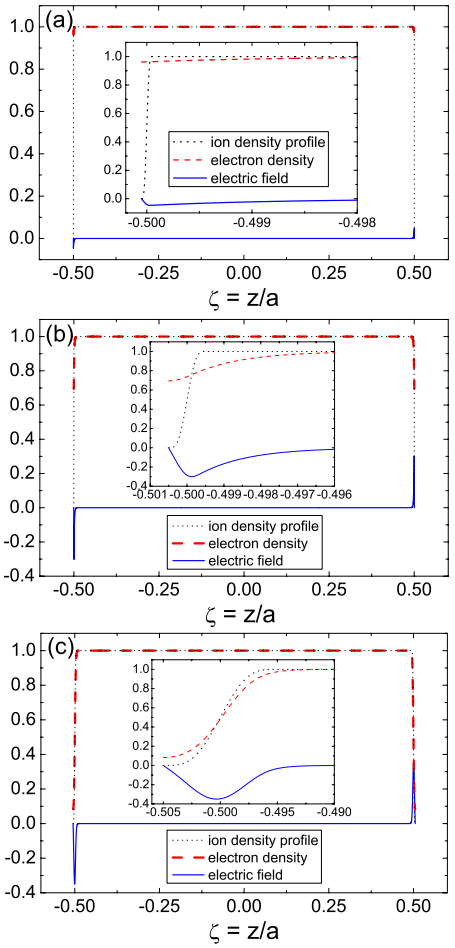

FIG. 2. (Color online) Exact numerical solutions of the static Eq. (12) for the electron density $n_s(\zeta)$ and the scaled electric field $\tilde{f}_s(\zeta)$ of a cold metal nanofilm with $A=10^{-6}$ and (a) $\tilde{\sigma}=10^{-4}$, (b) 10^{-3}, and (c) 10^{-2}; the global solutions and their behavior near the left-hand film boundary (insets). For the ion density of the boundary region, the smooth polynomial profile $g_4(x)$ is used (see Fig. 1).

2. Laser-heated/ionized films

For nanofilms heated by a strong pump-laser pulse up to the reference (longitudinal) electron temperature $T_\parallel=T_0\gg\varepsilon_F^{(0)}$, we can set $P_0=z_i n_{\rm ion}T_0$ so $P_s=n_s$ and $A=(l_D/a)^2$ with the conventional Debye length[41] $l_D=\sqrt{T_0/(4\pi e^2 z_i n_{\rm ion})}$. Again, after introducing the variables $\tilde{\zeta}=\zeta/\sqrt{A}$ and $\tilde{f}=f/\sqrt{A}$, we can rewrite Eq. (7) for laser-heated nanofilms as

$$\frac{dn_s}{d\tilde{\zeta}} + n_s \tilde{f}_s = 0, \quad \frac{d\tilde{f}_s}{d\tilde{\zeta}} = \Theta_i(\tilde{\zeta}\sqrt{A}) - n_s. \tag{13}$$

Hence, the normalization length in the new dimensionless variables now is the Debye length l_D instead of the film thickness a.

Typical values of the Debye length for films heated by a strong laser pulse are in the range of several tenths of a nanometer (for example, at $T_0=100$ eV and the respective bulk electron densities, it ranges from 0.15 nm for Be up to 0.78 nm for Cs). Hence, for a film with a thickness of 100 nm the parameter A is in the range of $10^{-6}-10^{-4}$, depending on the electron temperature and the metal species. For films with 10 nm in thickness, it is higher by two orders of magnitude ($10^{-4}-10^{-2}$). In this case, the Debye length and the diffuseness of the film edges may be of the same order. Note also that a film heated by a strong pump-laser field may be locally charged. This means that a fraction of the electrons can escape locally from the film during the action of the pump-laser pulse. If the neutralization time (which is of the order of $D/v_F \approx 10$ ps for the laser-focus diameter $D \sim 10$ μm, with v_F as the Fermi velocity) is longer than the delay between the pump pulse and the probe pulse, an outer-ionization degree $\eta = 1 - \int_{-\infty}^{+\infty} n(\zeta) d\zeta$ should be introduced to characterize the global lack of compensation of the positive and negative charges of the nanofilm. To take this into account, we must numerically solve Eq. (13) as a boundary-value problem with the boundary conditions $f_s(\mp\infty) = \mp \eta/2$, that is, $\tilde{f}_s(\mp\infty) = \mp \eta/(2\sqrt{A})$. Doing so we allow for the existence of an electron-density tail outside the ion core. Note that charged films can be described only with nonzero A. Due to Coulomb explosion of the charged film and the ensuing ion density, the Debye length for a charged film can be even higher than estimated above. On the other hand, the diffuseness of the film edge can also be higher than for a cold uncharged film as a result of Coulomb explosion. As examples, for charged laser-heated nanofilms with $A=10^{-4}$ and $\tilde{\sigma}=10^{-2}$, and also with $A=10^{-3}$ and $\tilde{\sigma}=10^{-1}$, solutions of the static Eq. (13) for the electron density $n_s(\zeta)$ and the electric field $f_s(\zeta)$ are presented in Figs. 3(a) and (b) and Figs 3(c) and (d), respectively, for various values of the outer-ionization degree η. These results show that in laser-heated nanofilms the role of the diffuseness of the film boundary is less essential than in cold metal nanofilms, at least if $\tilde{\sigma} \ll 1$. The outer-ionization degree may play a more significant role for the properties of the linear and nonlinear excitations of the plasma resonance due to the strong decrease in the electron density caused by outer ionization just near the film boundaries.

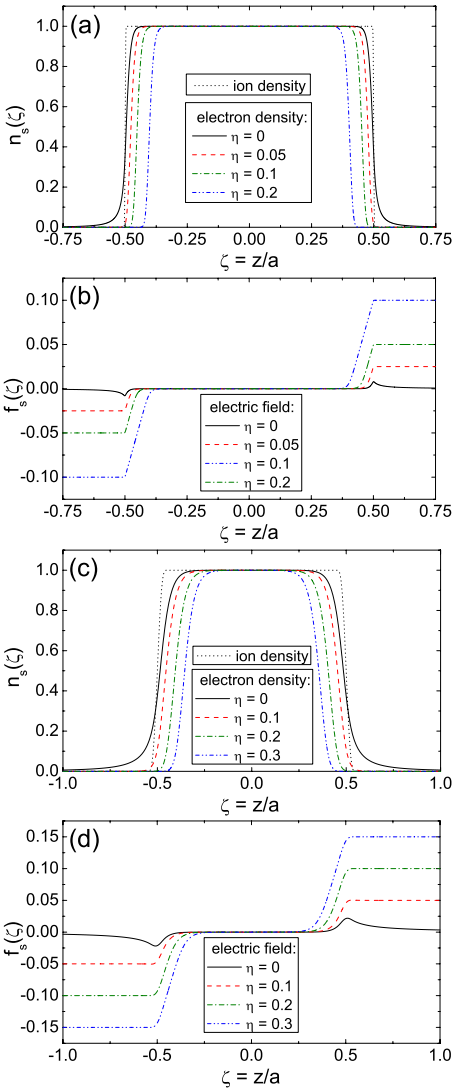

FIG. 3. (Color online) Exact numerical solutions of the static Eq. (13) for the electron density $n_s(\zeta)$ and the electric field $f_s(\zeta)$ of a laser-heated/ionized nanofilm with [(a) and (b)] $A=10^{-4}$ and $\tilde{\sigma}=10^{-2}$ and [(c) and (d)] with $A=10^{-3}$ and $\tilde{\sigma}=10^{-1}$ for various outer-ionization degrees η. For the ion density of the boundary region, the smooth polynomial profile $g_4(x)$ is used.

III. DYNAMICAL RESPONSE OF THE FILM: COLD NEUTRAL FILMS AT $A=0$

We start with the case when the parameter A of the film can be safely set to zero (or, equivalently, the quantum Debye screening length l_Q is set infinitely small with respect to the film-boundary thickness). This benchmark case could be relevant as a good approximation for cold neutral and thin metal nanofilms with sufficiently smooth boundary profiles. Whenever we are interested in analytical solutions of the hydrodynamic equations for films in the laser field, we will consider everywhere in this work the stationary approximation when the laser profile can be set to $f_L(\tau/\tau_p) \equiv 1$. In addition, perturbation theory with respect to the incoming laser field will be used to extract both the linear response of the film and the second-order and third-order nonlinearities. Disregarding the pressure terms in Eqs. (5a)–(5c), the set of dynamical equations in the approximation of $A=0$ for the neutral films is

$$\frac{\partial n}{\partial \tau} + \frac{\partial q}{\partial \zeta} = 0, \quad \frac{\partial f}{\partial \zeta} - \Theta_i(\zeta) + n = 0, \tag{14a}$$

$$n^2\left(\frac{\partial q}{\partial \tau}+\frac{\omega_p}{\omega}\gamma q\right)+2qn\frac{\partial q}{\partial \zeta}-q^2\frac{\partial n}{\partial \zeta}+\frac{n^3\omega_p^2}{\omega^2}\times\left\{\frac{1}{2}(e_L e^{-i\tau}+e_L^{\star}e^{i\tau})+f\right\}=0, \tag{14b}$$

where e_L is the dimensionless field amplitude defined below Eqs. (5a)–(5c). In the framework of perturbation theory, we will seek the solution for the electron density $n(\tau,\zeta)$ in the form

$$n(\tau,\zeta)=n_0(\zeta)+\mathrm{Re}\sum_{k=1}^{\infty}(e_L)^k e^{-ik\tau}n_k(\zeta). \tag{15}$$

The same is assumed for the electron current $q(\tau,\zeta)$ and the self-consistent electric field $f(\tau,\zeta)$ with Fourier coefficients $q_k(\zeta)$ and $f_k(\zeta)$, respectively. We will restrict ourselves to terms up to third order in the laser field. In the case of $A=0$, $n_0(\zeta)\equiv\Theta_i(\zeta)$ and $q_0(\zeta)=f_0(\zeta)=0$. In the perturbation series (15), it is assumed that the amplitudes n_k (as well as q_k and f_k) are independent of the laser field. In other words, we do not take into account possible nonlinear corrections dependent on $|e_L|^2$ to the amplitudes n_k, q_k, and f_k. These corrections do not occur in the equations for the amplitudes n_k, q_k, and f_k when they are assumed independent of the laser field. The latter is sufficient for our purposes. The corrections form their own system of equations, which, if necessary, could be considered separately from those that we solve.

It will be seen below that a necessary condition of expansion (15) to converge is that the film-boundary profile is sufficiently smooth at its end points. Moreover, the expansion parameter, which is the reduced laser electric field, should not exceed the threshold for nonlinear plasma instabilities such as wave breaking,[42–45] whose detailed description requires a kinetic approach.

At first glance, the condition of applicability of perturbation theory in this case is $e_L\ll 1$, that is, $E_0\ll E_a$, with $E_a=4\pi e z_i n_{\mathrm{ion}} a$. Even for nanofilms with thickness a of 10–100 nm, the field E_a is huge. In reality, as will be seen below, the applicability condition of perturbation theory is not connected with the film thickness but rather with the diffuseness of the film boundaries and should be written as $E_0\ll E_\sigma$, with $E_\sigma=4\pi e z_i n_{\mathrm{ion}}\sigma$. For $\sigma\sim 1$ nm, $E_\sigma\sim 10^{10}$ V/cm, which is still high enough. Note that the perturbation-theory condition $E_0\ll E_\sigma$ can be written in another equivalent form, namely, as $eE_0/(m_e\omega_p^2)\ll\sigma$. This means that the electron oscillation amplitude inside the film is smaller than the film-boundary thickness σ, which defines the minimal scale of inhomogeneity in the current case of $A=0$. Because the latter condition in a general form also defines the classical threshold for plasma wave breaking in the nonrelativistic regime,[44,45] the limiting external field E_σ for the applicability of perturbation theory and the threshold field for the occurrence of wave breaking are actually identical. In a detailed theory of wave breaking[42,43] the criterion for the wave-breaking threshold may somewhat differ from the classical one, but we always restrict ourselves to the range where wave breaking is still inessential.

A. Linear approximation

To all orders of perturbation theory ($k=1,2,3,\ldots$), Eqs. (14a) yield for the Fourier amplitudes

$$-ikn_k+\frac{dq_k}{d\zeta}=0, \tag{16a}$$

$$\frac{df_k}{d\zeta}+n_k=0 \tag{16b}$$

[the latter, Eq. (16b), is equivalent to the relation $-ikf_k-q_k=0$ if both the electron current and the dynamical part of the self-consistent electric field vanish far outside the film].

In linear approximation ($k=1$), Eq. (14b) becomes

$$\left(-i+\frac{\omega_p}{\omega}\gamma\right)q_1+\frac{n_0\omega_p^2}{\omega^2}(1+f_1)=0. \tag{17}$$

Its solution for the electron current amplitude $q_1(\zeta)$ is reminiscent of the plasma dielectric permittivity with account of the inhomogeneity of the ion density,

$$q_1=\frac{-i\frac{n_0\omega_p^2}{\omega^2}}{1-\frac{n_0\omega_p^2}{\omega^2}+i\gamma\frac{\omega_p}{\omega}}\equiv\frac{in_0}{n_0-\frac{\omega^2}{\omega_p^2}-i\gamma\frac{\omega}{\omega_p}}. \tag{18}$$

At each point of the film, the electron current is determined by the local plasma frequency $\omega_p^{(\mathrm{loc})}=\omega_p\sqrt{n_0(\zeta)}\equiv\omega_p\sqrt{\Theta_i(\zeta)}$, which depends on the local positive charge density of the ion background. Actually, this dependence is important only in the vicinity of the film edges.

In the dipole approximation, which is applicable to the description of the transverse electron dynamics of the film under our conditions, the linear electromagnetic response of the film is defined by its transverse dipole moment. The dimensionless dipole moment d_1 of the film at the fundamental laser frequency can be calculated as

$$d_1=-\int_{-(1+\tilde{\sigma})/2}^{(1+\tilde{\sigma})/2}n_1(\zeta)\zeta d\zeta\equiv\int_{-(1+\tilde{\sigma})/2}^{(1+\tilde{\sigma})/2}\frac{n_0(\zeta)d\zeta}{n_0(\zeta)-\frac{\omega^2}{\omega_p^2}-i\gamma\frac{\omega}{\omega_p}}, \tag{19}$$

where the integration is performed over the extent of the film including its diffuse boundaries, i.e., between the points, in which both our model ion density $n_0(\zeta)$ and the electron current $q_1(\zeta)$ vanish, the latter in accordance with Eq. (18). In the second step of Eq. (19), Eq. (16a) was used.

The film absorption cross section σ_{abs} is defined as the ratio of the laser energy absorbed per unit time over the incoming laser-energy flux density. For a finite laser-spot area S_L on the film surface (with typically $S_L>\pi\lambda^2$) and for the transverse electric-field component only acting on the film in our one-dimensional model, we write it in the form

$$\sigma_{\mathrm{abs}}=\sin^2\theta(a\omega_p/c)S_L\alpha, \tag{20}$$

where $\alpha=\tilde{\omega}\,\mathrm{Im}\,d_1$ is the *dimensionless* absorption coefficient, which is independent of the film thickness a. Here and below, we will use the dimensionless ratio $\tilde{\omega}\equiv\omega/\omega_p$.

For our model of the ion-density profile, the dimensionless absorption coefficient α can be rewritten as

$$\alpha = \frac{(1-\tilde{\sigma})\gamma\tilde{\omega}^2}{(1-\tilde{\omega}^2)^2+\gamma^2\tilde{\omega}^2} + \int_{-1/2}^{1/2} \frac{2\tilde{\sigma}\gamma\tilde{\omega}^2 g(x)dx}{[g(x)-\tilde{\omega}^2]^2+\gamma^2\tilde{\omega}^2}. \quad (21)$$

Here the first term comes from the bulk absorption and is independent of the edge profile, while the second term comes from the diffuse boundaries of the film. In the collisionless limit of $\gamma \to +0$ we obtain

$$\alpha = \tilde{\omega}(1-\tilde{\sigma})\pi\delta(1-\tilde{\omega}^2) + 2\tilde{\omega}\tilde{\sigma}\pi\int_{-1/2}^{1/2} \frac{g}{g'}\delta(g-\tilde{\omega}^2)dg$$

$$= \tilde{\omega}(1-\tilde{\sigma})\pi\delta(1-\tilde{\omega}^2) + \frac{2\pi\tilde{\sigma}\tilde{\omega}^3}{g'|_{g=\tilde{\omega}^2}}, \quad (22)$$

where $\delta(x)$ is the Dirac delta function. The second term results in nonzero collisionless absorption for $\tilde{\omega}<1(\omega<\omega_p)$. It is due to resonance absorption under the condition of a nonuniformly distributed ion-charge density from the maximal bulk density up to zero (in our model) in the diffuse film boundary of thickness σ. The competition between the two terms in Eq. (21) is determined by the ratio of the dimensionless relaxation constant γ and the relative thickness $\tilde{\sigma}$ of the film boundary. In the limit of $\tilde{\sigma} \to +0$ the collisionless contribution disappears.

Estimates of the dimensionless relaxation parameter γ can be made on the basis of the conventional electron-ion relaxation rates,[40] namely, for cold metal films (CF) $\gamma=\gamma^{\mathrm{CF}} \sim T_0/(\hbar\omega_p)$, while for hot laser-heated films (HF) $\gamma=\gamma^{\mathrm{HF}} \sim z_i^2 e^4 n_{\mathrm{ion}} L_C/(T_0^{3/2} m_e^{1/2}\omega_p)$, with $L_C \sim 10$ the Coulomb logarithm. For typical values of the metal plasmon energy $\hbar\omega_p \lesssim 10$ eV and for T_0 corresponding to room temperature or somewhat below, estimations show that typically $\gamma \sim 10^{-2}-10^{-3}$ for cold metal films. The same estimation is obtained for hot laser-heated films, if we assume $z_i \sim 1$, $n_{\mathrm{ion}} \sim 10^{22}$ cm^{-3} and $T_0 \sim 100$ eV. For this reason, in the following numerical calculations we will always set $\gamma=10^{-3}$ so that the film-boundary effects are not covered by the bulk contributions whose relative significance increases with increasing γ.

Figure 4(a) presents the results of a calculation of the absorption coefficient α for $\gamma=10^{-3}$ and $\tilde{\sigma}=10^{-2}$, and for the different edge profiles presented in Fig. 1 (for the frequency range of $10^{-2}<\tilde{\omega}<2$). For $\tilde{\omega}<1$, absorption is strongly enhanced by the diffuse-edge contribution compared with the step-like case of $\sigma=0$ (the dotted curve), and it is dependent on the edge profile. We observe a significant difference between the trapezoidal profile $g_1(x)$ on one hand and the various smooth profiles $g_i(x)$ $(i=2,3,4)$ on the other hand, which practically agree in the frequency range $0.1<\tilde{\omega}<1$ and result in a one-order-of-magnitude increase in absorption for our choice of the parameters $\tilde{\sigma}$ and γ.

The cross section for scattering off the film at the fundamental frequency (that is, for reflection of the incident radiation) can be written in a form similar to Eq. (20) as

$$\sigma_{\mathrm{scatt}(\omega)} = \beta_1 \sin^2\theta(\omega_p/c)^4 a^2\lambda^2 S_L w_1, \quad (23)$$

where $w_1=\tilde{\omega}^4|d_1|^2$ is the dimensionless dipole-radiation intensity at the fundamental laser frequency, which plays the role of the dimensionless scattered power, and β_1 is a numerical factor of the order of unity, which depends, in particular, on the angular range of detection. Similar to the absorption coefficient α, the quantity w_1 is defined so that it is independent of the film thickness a. The frequency dependence of the dimensionless scattered intensity w_1 is presented in Fig. 4(b). Because it is mainly determined by the real part of the dipole moment from Eq. (19), it is only negligibly affected by the edge diffuseness. At $\tilde{\sigma} \ll 1$, w_1 is well described by the standard Lorentz-type expression

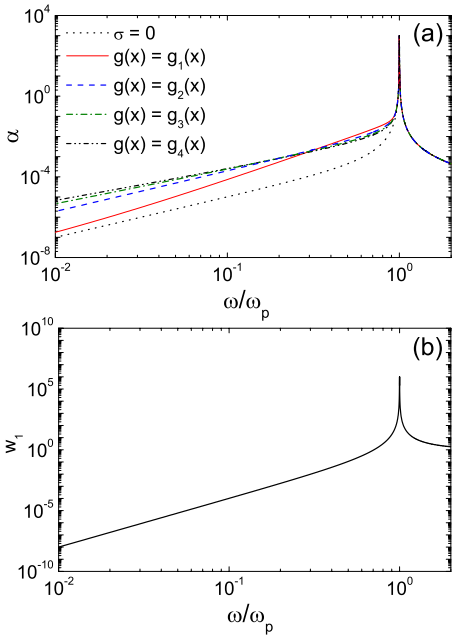

FIG. 4. (Color online) (a) The absorbed power α as a function of the laser frequency for the edge diffuseness $\tilde{\sigma}=10^{-2}$ and relaxation constant $\gamma=10^{-3}$, and for different edge profiles $g_i(x)$ (see Fig. 1), as compared with the case of $\sigma=0$ (the dotted curve); (b) the scattered power w_1, which is practically identical for all cases.

$$w_1 \approx \frac{\tilde{\omega}^4}{(1-\tilde{\omega}^2)^2+\gamma^2\tilde{\omega}^2}, \quad (24)$$

which is independent of $\tilde{\sigma}$ and the edge profile. It is shown here for later comparison with the corresponding dimensionless w_1 quantity for the case of $A \neq 0$ (see Sec. IV A).

B. Second-order and third-order approximations

Turning our attention to the nonlinear effects, we are mainly interested in the resonance-enhanced third-harmonic generation by nanofilms. When the laser frequency is near one third of the plasma frequency, the third-harmonic response of the film should exhibit resonance behavior. In the transverse dipole approximation applicable under our conditions, second-harmonic generation from nanofilms is missing. To calculate the third-harmonic response, we have to solve the perturbation-theory equations both to the second and to the third orders. In the case of $A=0$, which we consider now, the second-order equation for the electron current amplitude is

$$n_0^2\left(-2i+\frac{\gamma}{\tilde{\omega}}\right)q_2+n_0n_1\left(-i+\frac{\gamma}{\tilde{\omega}}\right)q_1+n_0q_1\frac{dq_1}{d\zeta}-\frac{q_1^2}{2}\frac{dn_0}{d\zeta}+\frac{1}{\tilde{\omega}^2}\left\{n_0^3f_2+\frac{3n_1n_0^2}{2}(1+f_1)\right\}=0. \tag{25}$$

With the help of Eqs. (16) and (18) we arrive at the solution

$$q_2=\frac{i\tilde{\omega}^2(n_0+2\tilde{\omega}^2+3i\gamma\tilde{\omega}-\gamma^2)n_0'}{(n_0-4\tilde{\omega}^2-2i\gamma\tilde{\omega})(n_0-\tilde{\omega}^2-i\gamma\tilde{\omega})^3}. \tag{26}$$

As expected, the second-order response of the film contains resonance denominators both at $\tilde{\omega}=\sqrt{n_0}$ and at $\tilde{\omega}=\frac{1}{2}\sqrt{n_0}$ [with $n_0(\zeta)\equiv\Theta_i(\zeta)$ in the case of $A=0$]. Moreover, it is proportional to the first derivative n_0' of the static electron density, that is, to the first derivative of the ion-charge density in this case. This implies that the second-order nonlinear response only differs from zero in the narrow ranges of the two diffuse boundaries of the film, where the ion density changes, and it vanishes everywhere in the bulk. This is also true for the third-order nonlinear response of the film (and to all higher orders). It means that the density gradient in the diffuse film edges is the only physical source of the harmonics in our model. On the other hand, for the trapezoidal profile $g_1(x)$ of the film boundary, the second-order current $q_2(\zeta)$ has discontinuities at $\zeta=\pm\frac{1}{2}(1\pm\tilde{\sigma})$, i.e., on the edges of the extended film boundaries. For this reason, the trapezoidal profile is questionable for a correct description of the second-order nonlinearity. To avoid this undesirable discontinuity, which will generate even stronger singularities in the higher-order nonlinear responses, the use of the smoother boundary profiles is preferable. For the second-order current $q_2(\zeta)$ to be continuous, it is sufficient to use the profiles $g_i(x)$ $(i=2,3,4)$ from Fig. 1, for which at least the first derivative vanishes at the edges of the extended film boundary.

The third-order perturbation-theory equation for the electron current in the case of $A=0$ is

$$n_0^2\left(-3i+\frac{\gamma}{\tilde{\omega}}\right)q_3+\left(n_0n_2+\frac{n_1^2}{4}\right)\left(-i+\frac{\gamma}{\tilde{\omega}}\right)q_1+n_0n_1\left(-2i+\frac{\gamma}{\tilde{\omega}}\right)q_2+\left(n_0q_2+\frac{n_1q_1}{2}\right)\frac{dq_1}{d\zeta}+n_0q_1\frac{dq_2}{d\zeta}-\frac{q_1^2}{4}\frac{dn_1}{d\zeta}-q_1q_2\frac{dn_0}{d\zeta}+\frac{1}{\tilde{\omega}^2}\left\{n_0^3f_3+\frac{3n_1n_0^2f_2}{2}+\left(\frac{3n_2n_0^2}{2}+\frac{3n_1^2n_0}{4}\right)(1+f_1)\right\}=0, \tag{27}$$

with the solution

$$q_3=\frac{3i\tilde{\omega}^3(3\tilde{\omega}+i\gamma)}{4}\left\{-\frac{(2n_0+2\tilde{\omega}^2+3i\gamma\tilde{\omega}-\gamma^2)n_0''}{(n_0-\tilde{\omega}^2-i\gamma\tilde{\omega})^4(n_0-4\tilde{\omega}^2-2i\gamma\tilde{\omega})(n_0-9\tilde{\omega}^2-3i\gamma\tilde{\omega})}+\frac{(8n_0^2-14\tilde{\omega}^2n_0-42\tilde{\omega}^4+3in_0\gamma\tilde{\omega}-81i\gamma\tilde{\omega}^3-5\gamma^2n_0+48\gamma^2\tilde{\omega}^2+9i\gamma^3\tilde{\omega})n_0'^2}{(n_0-\tilde{\omega}^2-i\gamma\tilde{\omega})^5(n_0-4\tilde{\omega}^2-2i\gamma\tilde{\omega})^2(n_0-9\tilde{\omega}^2-3i\gamma\tilde{\omega})}\right\}. \tag{28}$$

Compared with the second-order electron current q_2 [Eq. (26)], the third-order current amplitude contains an additional resonance denominator at $\tilde{\omega}=\frac{1}{3}\sqrt{n_0}$. The amplitude consists of two terms, which are proportional to n_0'' and to $n_0'^2$, respectively. On one hand, this leads to the conclusion, mentioned above, that the actual expansion parameter of the perturbation theory in the case of $A=0$ is not e_L as it seems from Eq. (15) but rather $e_L/\tilde{\sigma}$, that is, E_0/E_σ. On the other hand, for the third-order current $q_3(\zeta)$ to be continuous everywhere, the film-boundary profiles $g_3(x)$ and $g_4(x)$ from Fig. 1 must be used, for which at least the second derivative vanishes at the edges of the extended film boundary.

For the film that we consider, we write the cross section for scattering into the third harmonic in the form

$$\sigma_{\mathrm{scatt}(3\omega)}=\beta_3\sin^6\theta\left(\frac{3\omega_p}{c}\right)^4\left(\frac{E_0}{4\pi ez_in_{\mathrm{ion}}a}\right)^4a^2\lambda^2S_Lw_3, \tag{29}$$

where β_3 is a numerical factor of the order of unity depending on the angular range of detection of the third-harmonic radiation. The dynamics of the laser-film interaction is contained in the dimensionless quantity $w_3=(3\tilde{\omega})^4|d_3|^2$, which is the dimensionless dipole-radiation third-harmonic intensity, where d_3 is the nonlinear dipole-moment amplitude at three times the laser frequency,

$$d_3=-\int_{-(1+\tilde{\sigma})/2}^{(1+\tilde{\sigma})/2}n_3(\zeta)\zeta d\zeta=-\frac{\tilde{\omega}^3(3\tilde{\omega}+i\gamma)}{4}\int_{-(1+\tilde{\sigma})/2}^{(1+\tilde{\sigma})/2}\frac{(2n_0+2\tilde{\omega}^2+3i\gamma\tilde{\omega}-\gamma^2)n_0'^2d\zeta}{(n_0-\tilde{\omega}^2-i\gamma\tilde{\omega})^4(n_0-4\tilde{\omega}^2-2i\gamma\tilde{\omega})(n_0-9\tilde{\omega}^2-3i\gamma\tilde{\omega})^2}. \tag{30}$$

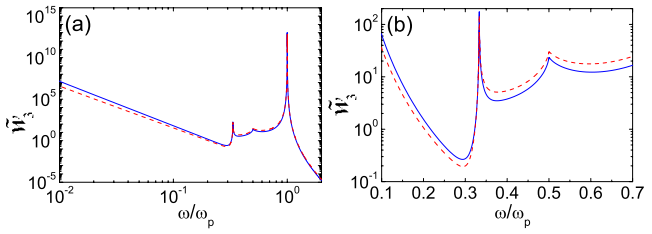

FIG. 5. (Color online) Universal frequency dependence of the third-harmonic intensity $\tilde{w}_3$ at $\gamma=10^{-3}$ and for the two smoothed edge profiles $g_3(x)$ (solid curve) and $g_4(x)$ (dashed curve) (see Fig. 1); (a) the global frequency dependence and (b) in the vicinity of the third-order resonance.

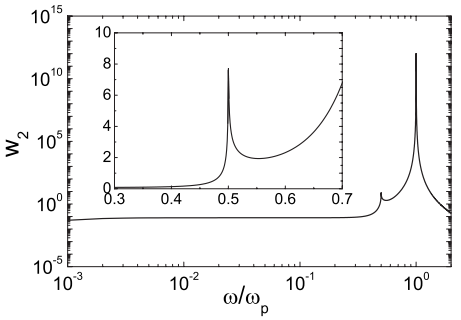

FIG. 6. Frequency dependence of the second-order harmonic response w_2 at $\gamma=10^{-3}$. The inset shows the region around the second-order resonance enlarged.

Again, in the first step Eq. (16a) was used followed by an integration by parts. The final result (30) was obtained with another integration by parts applied to the first term proportional to the second derivative of the static electron density $n_0''(\zeta)$ in the right-hand side of Eq. (28). This leads to the appearance of the square of the third-order resonance denominator. In both integrations by parts, the boundary terms vanish if the strongly smooth functions $g_3(x)$ or $g_4(x)$ are implied. Actually, the integration in Eq. (30) is only over the narrow range of the diffuse boundaries of the film. As a result, for fixed boundary profile and for fixed laser frequency, d_3 is proportional to $1/\tilde{\sigma}$ and w_3 is proportional to $1/\tilde{\sigma}^2$. Of course, this scaling is valid only under the condition $\tilde{\sigma} \gg \sqrt{A}$, i.e., only when the approximation $A=0$ is applicable. In other words, the reduced (and also dimensionless) third-harmonic intensity $\tilde{w}_3 \equiv \tilde{\sigma}^2 w_3$ does not depend on the film-boundary thickness for fixed boundary profile but may be different for different profiles and is therefore most convenient for comparing the frequency dependence of the third-harmonic radiation in different cases. In terms of the dimensionless quantity $\tilde{w}_3$, which is independent of the incident laser intensity, Eq. (29) can be rewritten as

$$\sigma_{\mathrm{scatt}(3\omega)}/S_L = 4.3 \times 10^{-23} \beta_3 \sin^6\theta (\lambda_p[\mathrm{nm}])^4 \times (I_0[10^{12}\ \mathrm{W/cm^2}])^2 (\lambda/\sigma)^2 \tilde{w}_3, \quad (31)$$

in which the dimensionless ratio $\sigma_{\mathrm{scatt}(3\omega)}/S_L$ on the left-hand side is the conversion efficiency of the incident radiation into the third harmonic. It can easily be estimated for given experimental parameters if $\tilde{w}_3$ is known. In Eq. (31), I_0 is the incident laser intensity, λ is the laser wavelength, and $\lambda_p = 2\pi c/\omega_p$ is the nominal (bulk) plasma resonance wavelength. Note that not only the quantity $\tilde{w}_3$ but also the entire right-hand side of Eq. (31) does not exhibit any explicit dependence on the film thickness a, in contrast to linear absorption and linear scattering at the fundamental laser frequency [cf. Eq. (31) with Eqs. (20) and (23)].

For the reduced third-harmonic intensity $\tilde{w}_3$, the results of the integration are presented in Fig. 5. Figure 5(a) shows the global frequency dependence of the reduced third-harmonic intensity calculated with the smoothed boundary profiles $g_i(x)$ $(i=3,4)$, while Fig. 5(b) exhibits the vicinity of the third-order resonance. Near the third-order nonlinear plasma resonance at $3\omega \approx \omega_p$, the frequency dependence of the third-harmonic intensity demonstrates resonance behavior, which is qualitatively similar for the two edge profiles. Note also that there is a weak but noticeable singularity in the third-harmonic intensity near the frequency $\omega=\omega_p/2$ (when $3\omega \approx \frac{3}{2}\omega_p$). The smoother the edge profile, the weaker the singularity near this resonance. The weak singularity is due to the fact that the integrand of Eq. (30) contains only the first power of the second-order resonance denominator. In consequence, this singularity in the frequency dependence of w_3 after integration over the edge profile is only logarithmic. The same is also true for the second-order dipole response [Eq. (26)]. In the dipole approximation, the nanofilm does not radiate at the second harmonic because the corresponding dipole moment vanishes (but the second harmonic can be present in the self-consistent electric field inside the nanofilm). However, for purposes of comparison we may calculate the second-order harmonic response $w_2=(2\tilde{\omega})^4|d_2|^2$, with the dipole moment defined as $d_2=-\int_{-(1+\tilde{\sigma})/2}^{0} n_2(\zeta)\zeta d\zeta$, i.e., by integrating only over one (the left) boundary of the film. Therefore, w_2 so defined has a universal frequency behavior with only a logarithmic singularity near the second-order resonance frequency at $2\omega \approx \omega_p$. The result for w_2 so defined is presented in Fig. 6. Note that w_2, as well as d_2, do not depend at all on the film-boundary profile. Hence, second-harmonic generation is absent (in the dipole approximation) even with nonsymmetric film boundaries.

The results presented in Figs. 5 and 6 for $\tilde{w}_3$ and w_2, respectively, exhibit the universal frequency dependence of the third-order and the second-order responses of the film, which are independent of the incident laser intensity, the film thickness, the film-boundary thickness, and the nominal film plasma frequency (or wavelength). To estimate the third-harmonic efficiency according to Eq. (31), some of these parameters should be specified. For example, if we assume $n_i z_{\mathrm{ion}}=2\times10^{22}\ \mathrm{cm^{-3}}$, then $\lambda_p=242$ nm (with $\hbar\omega_p=4.8$ eV). For a laser operating at the wavelength $\lambda \approx 3\lambda_p$ with intensity $I_0=10^{14}\ \mathrm{W/cm^2}$ and for a film with boundary thickness $\sigma=1$ nm, we obtain from Eq. (31) that $\sigma_{\mathrm{scatt}(3\omega)}/S_L \approx 9.8\times10^{-6}\tilde{w}_3$ (to be specific, we assumed $\beta_3=0.1$ and $\sin^2\theta=0.5$). In view of Fig. 5(b), this implies that the conversion efficiency to the third harmonic in a wide range near the third-order resonance for these parameters is of the order of $10^{-4\pm1}$. This value is independent of the film thickness a, which may be arbitrary provided that $a \ll \lambda$. However, the above results are only exact in the case of $A=0$, which was

considered in this section. For $A \neq 0$, the film thickness a may be important.

IV. DYNAMICAL RESPONSE OF THE FILM: COLD NEUTRAL AND HOT CHARGED FILMS AT NONZERO A

Since the film parameter A is always quite small, one might expect that a nonzero value of A will only induce small corrections to the solution with $A=0$ presented in Sec. III, at least in the case of cold neutral metal films. However, whether or not this statement is correct depends on the intensity of the incident laser field. In the hydrodynamic Eqs. (5a)–(5c), we can perform a scaling transformation through the definitions $\tilde{\zeta}=\zeta/\sqrt{A}$, $\tilde{f}=f/\sqrt{A}$, $\tilde{q}=q/\sqrt{A}$, and $\tilde{e}_L=e_L/\sqrt{A}$. Then, the set of hydrodynamic equations can be rewritten in the form

$$\frac{\partial n}{\partial \tau}+\frac{\partial \tilde{q}}{\partial \tilde{\zeta}}=0, \quad \frac{\partial \tilde{f}}{\partial \tilde{\zeta}}-\Theta_i(\tilde{\zeta}\sqrt{A})+n=0, \tag{32a}$$

$$n^2\left(\frac{\partial \tilde{q}}{\partial \tau}+\frac{\gamma}{\tilde{\omega}}\tilde{q}\right)+2\tilde{q}n\frac{\partial \tilde{q}}{\partial \tilde{\zeta}}-\tilde{q}^2\frac{\partial n}{\partial \tilde{\zeta}} + \frac{n^2}{\tilde{\omega}^2}\left\{\frac{\partial P}{\partial \tilde{\zeta}}+\frac{n}{2}(\tilde{e}_L e^{-i\tau}+\tilde{e}_L^{\star}e^{i\tau})+n\tilde{f}\right\}=0, \tag{32b}$$

$$n^2\frac{\partial P}{\partial \tau}+n\tilde{q}\frac{\partial P}{\partial \tilde{\zeta}}+3nP\frac{\partial \tilde{q}}{\partial \tilde{\zeta}}-3\tilde{q}P\frac{\partial n}{\partial \tilde{\zeta}}=0, \tag{32c}$$

in which the parameter A has been completely eliminated (except for the argument of the ion-density function used in the static solution). This transformation means that the normalization length in the new dimensionless variables is the Debye screening length (the quantum length l_Q or the classical length l_D for cold or hot nanofilms, respectively), as was the case in the scaled static Eqs. (12) and (13). In Eqs. (32a)–(32c), we consider only the stationary approximation, assuming for the laser profile function the condition $f_L(\tau/\tau_p)=1$. In the framework of perturbation theory, we will now seek the solution for the electron density $n(\tau,\tilde{\zeta})$ in the form

$$n(\tau,\tilde{\zeta})=n_0(\tilde{\zeta})+\mathrm{Re}\sum_{k=1}^{\infty}(\tilde{e}_L)^k e^{-ik\tau}\tilde{n}_k(\tilde{\zeta}), \tag{33}$$

and the same expansions are assumed for all other variables $P(\tau,\tilde{\zeta})$, $\tilde{q}(\tau,\tilde{\zeta})$, and $\tilde{f}(\tau,\tilde{\zeta})$, with Fourier coefficients $P_k(\tilde{\zeta})$, $\tilde{q}_k(\tilde{\zeta})$, and $\tilde{f}_k(\tilde{\zeta})$, respectively. As before, we will restrict ourselves to terms up to the third order. In the case $A\neq 0$, we have $\tilde{q}_0(\tilde{\zeta})=0$, $n_0(\tilde{\zeta})=n_s(\tilde{\zeta})$, $P_0(\tilde{\zeta})=P_s(\tilde{\zeta})$, and $\tilde{f}_0(\tilde{\zeta})=\tilde{f}_s(\tilde{\zeta})$, with the solutions of the static Eqs. (12) or (13) for cold or laser-heated films, respectively, on the right-hand sides. The electron-density amplitudes n_k and the electron-current amplitudes q_k of the perturbation expansion (15) for $A=0$ and those of series (33) for $A\neq 0$ are related by $\tilde{n}_k=A^{k/2}n_k$ and $\tilde{q}_k=A^{(k-1)/2}q_k$. As before, to all orders of perturbation theory ($k=1,2,3,\ldots$) Eq. (32a) yields

$$-ik\tilde{n}_k+\frac{d\tilde{q}_k}{d\tilde{\zeta}}=0, \quad \frac{d\tilde{f}_k}{d\tilde{\zeta}}+\tilde{n}_k=0 \tag{34}$$

[again with the equivalent replacement of the second Eq. (34) by relation $-ik\tilde{f}_k-\tilde{q}_k=0$].

It should be noted that perturbation theory is quite different in this case from the previous case $A=0$ [see Eq. (15)]. The reason is that the latter cannot be obtained as the limiting case of $A\to+0$ from Eq. (33). The expansion parameter of this new perturbation expansion is $\tilde{e}_L$, so it is formally applicable under the condition $E_0 \ll E_a\sqrt{A}$, that is, under the condition $E_0 \ll E_l$, with $E_l=4\pi e z_i n_{\mathrm{ion}} l_Q$ or $E_l=4\pi e z_i n_{\mathrm{ion}} l_D$ for cold or laser-heated films, respectively. Again, this condition can be rewritten in the form of $eE_0/(m_e\omega_p^2)\ll l_Q$ or $eE_0/(m_e\omega_p^2)\ll l_D$, respectively. Hence, again the applicability limit E_l of perturbation theory also plays the role of the classical wave-breaking threshold[44,45] for the case of $A\neq 0$. Note that the electric field E_l is independent of the film dimensions and depends only on the bulk ion density and the film temperature (in the case of hot laser-heated films). In the limit of $A\to+0$ (where formally l_Q or l_D vanish), the range of applicability of this perturbation expansion goes to zero. On the other hand, in the range of $E_a\sqrt{A}\ll E_0\ll E_\sigma$ we retrieve the expansion considered in Sec. III under the assumption of $A=0$ (for neutral films).

Below, we will assume that the condition $\tilde{e}_L\ll 1$ is met. Despite the extreme smallness of A, especially in cold metal films, the reference electric field E_l is of the order of 10^8 V/cm for cold metal nanofilms, and it may be up to two orders of magnitude higher for laser-heated/ionized nanofilms. So, the actual range of applicability of this perturbation expansion includes laser fields of moderate intensity, which we will consider from now on.

A. Linear approximation

The equations for the first-order amplitudes in expansion (33) for the electron current and the pressure can be derived from Eqs. (32b) and (32c), and they are

$$\left(-i+\frac{\gamma}{\tilde{\omega}}\right)\tilde{q}_1+\frac{1}{\tilde{\omega}^2}\left\{\frac{dP_1}{d\tilde{\zeta}}+n_0(1+\tilde{f}_1)+\tilde{n}_1\tilde{f}_0\right\}=0,$$

$$-in_0^2P_1+\tilde{q}_1n_0\frac{dP_0}{d\tilde{\zeta}}+3P_0n_0\frac{d\tilde{q}_1}{d\tilde{\zeta}}-3\tilde{q}_1P_0\frac{dn_0}{d\tilde{\zeta}}=0, \tag{35}$$

while the static equation now reads $dP_0/d\tilde{\zeta}=-n_0\tilde{f}_0$. Equations (35) can be reduced to a single second-order differential equation for the first-order electron current amplitude $\tilde{q}_1$, namely, to the equation

$$\frac{3P_0}{n_0}\frac{d^2(i\tilde{q}_1)}{d\tilde{\zeta}^2}-\frac{d(i\tilde{q}_1)}{d\tilde{\zeta}}\left\{3\tilde{f}_0+\frac{6P_0}{n_0^2}\frac{dn_0}{d\tilde{\zeta}}\right\} - i\tilde{q}_1\left\{\frac{d}{d\tilde{\zeta}}\left(\tilde{f}_0+\frac{3P_0}{n_0^2}\frac{dn_0}{d\tilde{\zeta}}\right)+n_0-\tilde{\omega}^2-i\gamma\tilde{\omega}\right\}=n_0. \tag{36}$$

This equation can be further simplified in the cases of cold

metal films where $P_0=n_0^{5/3}$ and of hot laser-heated films where $P_0=n_0$. The corresponding equations are, respectively,

$$3n_0^{2/3}\frac{d^2(i\tilde{q}_1)}{d\tilde{\zeta}^2}+\frac{3}{5}\tilde{f}_0\frac{d(i\tilde{q}_1)}{d\tilde{\zeta}}+i\tilde{q}_1\left(\frac{4}{5}\frac{d\tilde{f}_0}{d\tilde{\zeta}}-n_0+\tilde{\omega}^2+i\gamma\tilde{\omega}\right)-n_0=0, \tag{37a}$$

$$3\frac{d^2(i\tilde{q}_1)}{d\tilde{\zeta}^2}+3\tilde{f}_0\frac{d(i\tilde{q}_1)}{d\tilde{\zeta}}+i\tilde{q}_1\left(2\frac{d\tilde{f}_0}{d\tilde{\zeta}}-n_0+\tilde{\omega}^2+i\gamma\tilde{\omega}\right)-n_0=0. \tag{37b}$$

In the case of cold metal films, Eq. (37a) should be solved with the boundary conditions $\tilde{q}_1[\pm(1+\tilde{\sigma})/(2\sqrt{A})]=0$, corresponding to the electron current vanishing everywhere outside the film. In order to be compatible with the case of $A=0$ [see Eq. (19)], the dipole-moment amplitude d_1 at the fundamental laser frequency should be defined by

$$d_1=-\sqrt{A}\int_{-(1+\tilde{\sigma})/(2\sqrt{A})}^{(1+\tilde{\sigma})/(2\sqrt{A})}\tilde{n}_1(\tilde{\zeta})\tilde{\zeta}d\tilde{\zeta}=-\sqrt{A}\int_{-(1+\tilde{\sigma})/(2\sqrt{A})}^{(1+\tilde{\sigma})/(2\sqrt{A})}i\tilde{q}_1(\tilde{\zeta})d\tilde{\zeta},$$

with the same definitions for the scattered power w_1 and the film absorption α as before. In the case of hot and charged laser-heated films, the boundary conditions to Eq. (37b) should be formally taken as $\tilde{q}_1(\pm\infty)=0$, assuming that the electron cloud vanishes far away from the film. Correspondingly, the dipole-moment amplitude should be defined as $d_1=-\sqrt{A}\int_{-\infty}^{+\infty}i\tilde{q}_1(\tilde{\zeta})d\tilde{\zeta}$. Calculated results for the scattered intensity w_1 and the film absorption α are presented and discussed in Secs. IV A 1 and IV A 2 for cold metal films and hot laser-ionized films, respectively.

1. Cold metal films

Figure 7 shows results for a relatively thick cold neutral metal nanofilm with $A=10^{-7}$. The calculations were carried out with the smooth film-boundary profile $g_4(x)$. The panels from (a) to (f) of Fig. 7 correspond to increasing values of the reduced thickness $\tilde{\sigma}$ of the film boundary. For sufficiently sharp film boundary with $\tilde{\sigma}\leq 10^{-3}$, the calculations show that both the scattered intensity w_1 and the film absorption α are the same as in the benchmark case of $A=0$ and $\tilde{\sigma}=0$ [see Fig. 4(a)]. Then, for $\tilde{\sigma}=1.5\times10^{-3}$ [panel (a)], a small splitting of the plasma resonance near $\tilde{\omega}=1$ already takes place. With $\tilde{\sigma}$ further increasing to 3×10^{-3} [panel (b)], the left peak is shifted to lower frequency. As a result, in the frequency range below the plasma resonance frequency, the frequency dependence of the film absorption is qualitatively modified with increasing $\tilde{\sigma}$. Namely, more and more additional absorption resonances appear. While for $\tilde{\sigma}=3\times10^{-3}$ [panel (b)] only one additional absorption resonance is present, a lot of quasiequally spaced absorption resonances occur for $\tilde{\sigma}=3\times10^{-2}$ [panel (e)] and especially for $\tilde{\sigma}=10^{-1}$ [panel (f)]. The film absorption strongly oscillates upon variation in the laser frequency. The absorption averaged over these oscillations is in accordance with that obtained in Sec. III A in the approximation of $A=0$. In the latter case, a smooth absorption curve was obtained, with magnitude

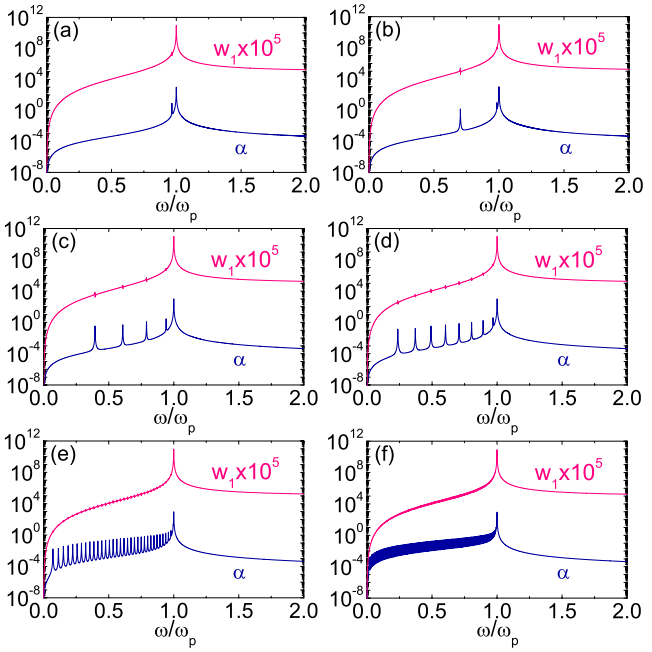

FIG. 7. (Color online) Frequency dependence of the absorption α and the scattered intensity w_1 for a neutral cold metal film with $A=10^{-7}$, $\gamma=10^{-3}$, and with $\tilde{\sigma}$ equal to (a) 1.5×10^{-3}, (b) 3×10^{-3}, (c) 6×10^{-3}, (d) 10^{-2}, (e) 3×10^{-2}, and (f) 10^{-1}.

much higher than for $\tilde{\sigma}=0$ [Fig. 4(a)]. For $A\neq0$, however, the evolution of the absorption curve with decreasing film-boundary thickness is qualitatively different from the case of $A=0$. For intermediate film-boundary thickness [panels (c) and (d) in Fig. 7], a set of well-resolved quasiequally spaced absorption peaks develops on top of the absorption curve for $\tilde{\sigma}=0$. On the other hand, for $A=10^{-7}$ no visible change in absorption is observed above the plasma resonance frequency. Also, the scattered intensity w_1 practically remains the same as in the case of $\tilde{\sigma}=0$. This is due to the smallness of the imaginary part of the dipole-moment amplitude d_1 with respect to its real part for the considered value of $A=10^{-7}$.

These main features remain the same for thinner nanofilms with $A=10^{-5}$ (Fig. 8). The absorption resonances below the plasma resonance frequency now appear for higher values (approximately one order of magnitude) of the reduced thickness $\tilde{\sigma}$ of the film boundary. Besides, with increasing film-boundary thickness $\tilde{\sigma}$ these resonances also appear in the scattered intensity w_1 [see panels (c)–(f) of Fig. 8] because the orders of magnitude of the real and the imaginary parts of the dipole-moment amplitude d_1 near the absorption resonances are now comparable. The most visible difference compared with the case of $A=10^{-7}$ is the appearance in the absorption α of a regularly spaced palisade of resonances *above* the plasma resonance frequency, especially for small values of the reduced film-boundary thickness $\tilde{\sigma}$, for which the low-frequency absorption resonances have not yet appeared. With increasing $\tilde{\sigma}$, this tight resonance structure gradually disappears. The resonances above the plasma frequency can be interpreted[26] as bulk-plasma waves resonantly excited in a whole thin metal film like in a capacitor.

Figures 7 and 8 show that with increasing film-boundary thickness $\tilde{\sigma}$ the low-frequency cutoff for the extra absorption

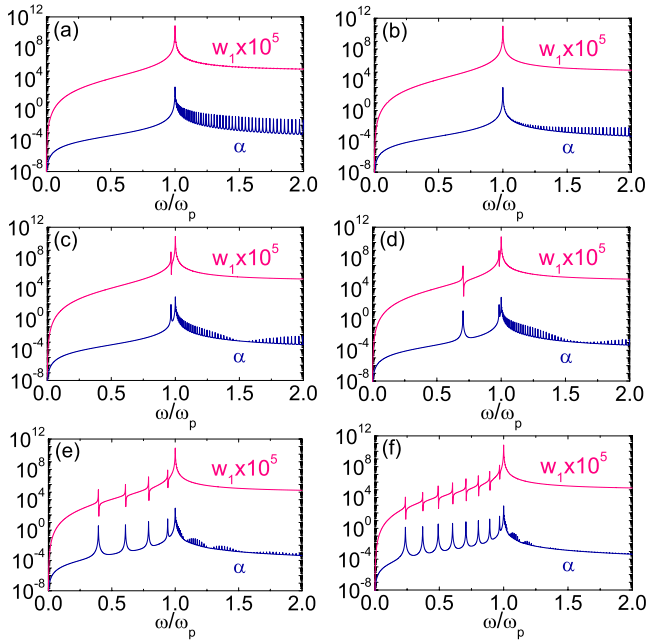

FIG. 8. (Color online) Same as Fig. 7 but for $A=10^{-5}$, $\gamma=10^{-3}$, and $\tilde{\sigma}$ equal to (a) 3×10^{-3}, (b) 10^{-2}, (c) 1.5×10^{-2}, (d) 3×10^{-2}, (e) 6×10^{-2}, and (f) 10^{-1}.

lines (below the bulk-plasma resonance) moves to lower and lower frequencies. It is important to note that this behavior correlates well with the decrease in the static electron density in the film-boundary region (see the insets of Fig. 2). This implies that in the immediate film-boundary region plasma oscillations of the electrons are formally possible with resonance frequencies that become lower and lower as the film-boundary thickness increases due to the decrease in the plasma frequency with decreasing density. Indeed, in this narrow film range where both the electron and the ion density are inhomogeneous, the discrete spectrum of the plasma eigenfrequencies should exhibit a spacing inversely proportional to the film-boundary thickness. These electron oscillations in the low-frequency domain (with respect to the bulk-plasma resonance) effectively occur only in the range of the film boundaries. Thus, the origin of the extra absorption resonances is directly connected with the spatial dependence of the solutions of Eq. (37a) for the electron current amplitude $\tilde{q}_1(\zeta)$.

To confirm this hypothesis, examples of the solutions of this equation are presented in Fig. 9 for two values of the laser frequency, one below and the other one above the plasma resonance, $\tilde{\omega}=0.6$ [panels (a), (b), (e), and (f)] and $\tilde{\omega}=1.4$ [panels (c), (d), (g), and (h)], and for two values of the parameter A, $A=10^{-7}$ [panels (a)–(d)] and $A=10^{-5}$ [panels (e)–(h)] for a nanofilm with $\tilde{\sigma}=10^{-2}$ and $\gamma=10^{-3}$. If the laser frequency is below the nominal (bulk) plasma resonance frequency, the electron current amplitude $\tilde{q}_1(\zeta)$ (both its real and its imaginary part) is almost constant inside the film while undergoing rapid change very close to its boundary. The variation in the electron current in this narrow range may be either oscillatory [see the insets of panels (a) and (b) of Fig. 9] or monotonic [see panels (e) and (f) of Fig. 9]. The latter case corresponds to Fig. 8(b), in which extra low-frequency absorption lines have not yet appeared. On the other hand, the oscillatory dependence of the electron current amplitude inside the film boundary appears to be correlated with the existence of the resonance modes where the extended film boundary acts like a resonator. For an example, compare panels (a) and (b) of Fig. 9 corresponding to the case of film with $A=10^{-7}$ and $\tilde{\sigma}=10^{-2}$ with Fig. 7(d). The fact that the frequency distance between the low-frequency absorption lines reduces with increasing boundary thickness $\tilde{\sigma}$ supports this interpretation.

In contrast to low frequencies, for frequencies above the plasma resonance the electron-current amplitude $\tilde{q}_1(\zeta)$ strongly oscillates over the entire extent of the film. This can be seen from Fig. 9 [panels (c), (d), (g), and (h)] for the laser frequency $\tilde{\omega}=1.4$, as well as in general from Eq. (37a), which has oscillatory solutions for $\tilde{\omega}>1$. From the latter, it is clear that the spatial period of the electron current oscillations in relative units is $\Delta\tilde{\zeta}\sim1$, so that $\Delta z\sim l_Q$ and the number of oscillations of the electron current in the film with thickness a is of the order of $a/l_Q=1/\sqrt{A}$. Again, drawing the

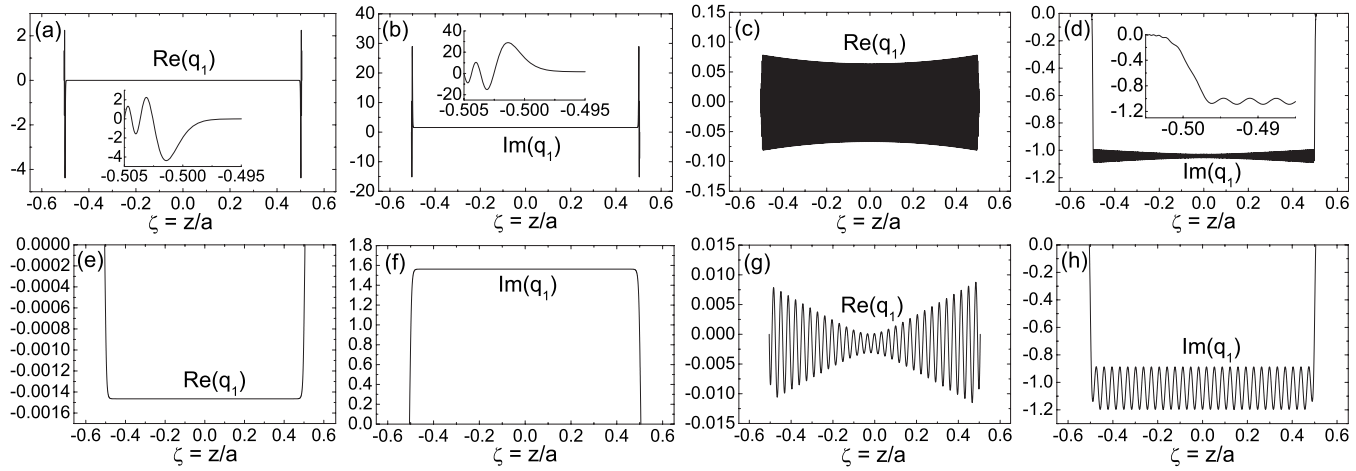

FIG. 9. Examples of solutions of Eq. (37a) for the spatial dependence of the real and imaginary parts of $\tilde{q}_1\equiv q_1$ at [(a), (b), (e), and (f)] $\tilde{\omega}=0.6$ and [(c), (d), (g), and (h)] $\tilde{\omega}=1.4$ for a neutral cold metal nanofilms with $\gamma=10^{-3}$, $\tilde{\sigma}=10^{-2}$, [(a)–(d)] $A=10^{-7}$, and [(e)–(h)] $A=10^{-5}$. Insets on the panels (a), (b), and (d) exhibit the fine structure of these solutions near the left film boundary.

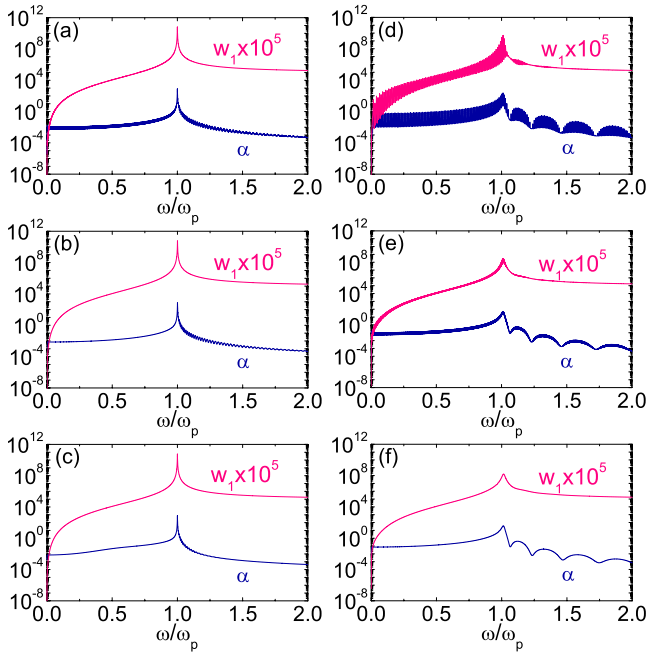

FIG. 10. (Color online) Frequency dependence of the absorption α and the scattered intensity w_1 for a neutral ($\eta=0$) laser-heated film with $\gamma=10^{-3}$, [(a)–(c)] $A=10^{-5}$ and [(d)–(f)] $A=10^{-3}$, and with $\tilde{\sigma}$ equal to [(a) and (d)] 10^{-3}, [(b) and (e)] 10^{-2}, and [(c) and (f)] 10^{-1}.

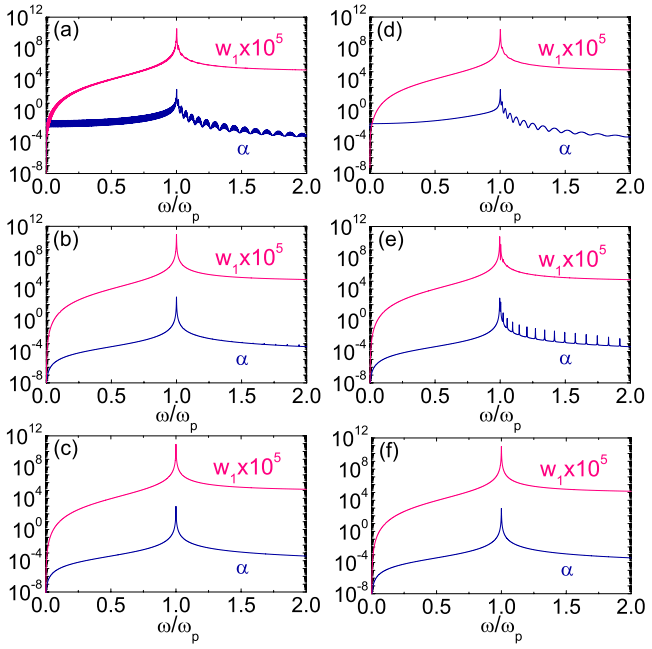

FIG. 11. (Color online) Frequency dependence of the absorption α and the scattered intensity w_1 for a hot laser-heated film with $\gamma=10^{-3}$ and $A=10^{-4}$, with [(a)–(c)] $\tilde{\sigma}=10^{-3}$ and [(d)–(f)] $\tilde{\sigma}=10^{-1}$, and with outer-ionization degree [(a) and (d)] $\eta=0$, [(b) and (e)] 0.05, and [(c) and (f)] 0.1.

analogy with a whole film as a resonator[26] we can conclude that, for laser frequencies above the plasma resonance, the frequency distance between the extra absorption lines (if they occur) reduces with increasing film thickness a. In this case, the thickness of the film boundary, that is, the parameter $\tilde{\sigma}$, plays only a minor role. For sufficiently thick films, these resonances—even though formally they continue to exist—will merge and disappear in practice. This will happen when their frequency separation becomes comparable with or smaller than their width, which is defined by the small parameter γ. This seems to be the case for Fig. 7 for the film with $A=10^{-7}$, where the resonances above the plasma frequency are completely missing, in contrast to the case of Fig. 8 for the film with $A=10^{-5}$.

2. Laser-heated/ionized films

The results of calculations for the benchmark case of a neutral laser-heated nanofilm are shown in Fig. 10 for two different values of the parameter A: $A=10^{-5}$ [panels (a)–(c)] and $A=10^{-3}$ [panels (d)–(f)]. Panels (a)–(c) for $A=10^{-5}$ and (d)–(f) for $A=10^{-3}$ correspond to increasing values of the reduced thickness $\tilde{\sigma}$ of the film boundary. The calculations were done with the smooth film-boundary profile $g_4(x)$. The results show that there are no additional absorption resonances in this case, in contrast to the previous case of a cold metal nanofilm. Moreover, only insignificant changes in both the absorption α and the scattered intensity w_1 occur with increasing $\tilde{\sigma}$. This qualitative difference from the case of cold metal films may be a consequence of the presence of the Debye tail of the electron density far away from the film boundary in hot neutral films (see Fig. 3). More importantly, absorption is considerably higher for low frequencies compared with the case of cold metal films and demonstrates a very slow dependence on frequency for $\tilde{\omega}<1$, cf. Fig. 10 with Figs. 7 and 8. Also, with A increasing from 10^{-5} to 10^{-3}, absorption increases in the low-frequency range and the plasma resonance at $\tilde{\omega}=1$ becomes smoother. This indicates that with decreasing film thickness a (or with increasing Debye length l_D, which may be caused by increasing film temperature), the plasma resonance is broadened. A similar effect is known for cold nanoclusters from the solution of the kinetic Vlasov equation.[14] The physical reason for the broadening of the Mie resonance with decreasing cluster radius is Landau damping in a finite system. Figure 10 shows that a similar effect takes place for the plasma resonance in nanofilms and that it can be described already in the hydrodynamic approximation.

Figure 11 illustrates the consequences when the film acquires a net charge due to outer ionization. It shows the frequency dependence of the absorption α and the scattered intensity w_1 for a charged laser-heated nanofilm with $\gamma=10^{-3}$ and $A=10^{-4}$, with [(a)–(c)] $\tilde{\sigma}=10^{-3}$ and [(d)–(f)] $\tilde{\sigma}=10^{-1}$, and with outer-ionization degree [(a) and (d)] $\eta=0$, [(b) and (e)] 0.05, and [(c) and (f)] 0.1. The results for a neutral film are presented for comparison [panels (a) and (d)]. The drastic difference between the neutral films and the charged films in the frequency dependence of the absorption in the range of low frequencies $\tilde{\omega}<1$ is clearly seen. Already for 5% ionization, absorption at low frequencies drops by many orders of magnitude. When the outer-ionization degree further increases up to 0.1 [panels (c) and (f) of Fig. 11] and to 0.15 (this was checked in calculations but is not shown), no additional changes are observed neither in the absorption

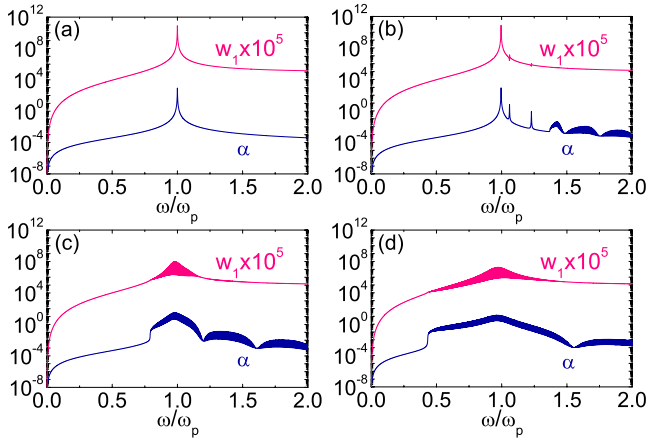

FIG. 12. (Color online) Frequency dependence of the absorption α and the scattered intensity w_1 for a charged ($\eta=0.1$) hot laser-heated film with $\gamma=10^{-3}$ and $\tilde{\sigma}=10^{-2}$, and with (a) $A=10^{-4}$, (b) 10^{-3}, (c) 3×10^{-3}, and (d) 10^{-2}.

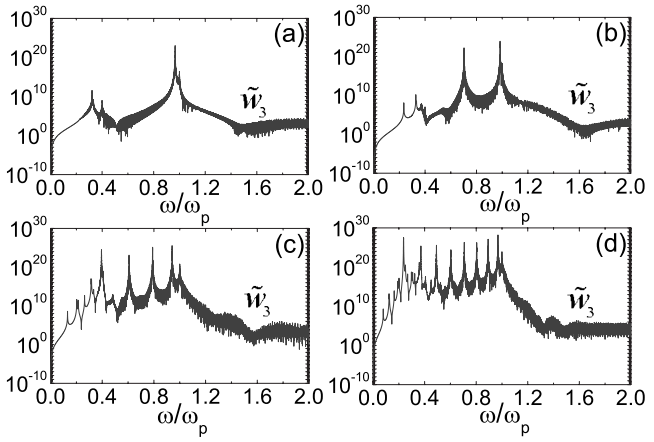

FIG. 13. Frequency dependence of the third-harmonic intensity $\tilde{w}_3$ for a neutral cold metal film with $A=10^{-7}$, $\gamma=10^{-3}$, and with $\tilde{\sigma}$ equal to (a) 1.5×10^{-3}, (b) 3×10^{-3}, (c) 6×10^{-3}, and (d) 10^{-2}.

nor in the scattered intensity, except for a weak palisade of resonances above the plasma resonance frequency in panel (e) of Fig. 11.

If a hot laser-heated film becomes noticeably charged, absorption at low frequencies becomes quite different from that for a neutral hot film. At the same time, it becomes quite similar to that of a cold neutral metal film if we ignore the extra absorption lines (cf. Fig. 11 with Figs. 7 and 8). This change in the low-frequency absorption between the neutral and the charged hot laser-heated films is the consequence of the differences in the quasiequilibrium electron-density distributions; in a neutral hot film the electron density extends beyond the film boundary and forms the Debye tail outside the film, while in a charged film all residual electrons are trapped inside the film, and the density on the film boundary is strongly reduced (see Fig. 3). For this reason, boundary effects in the laser-film interaction are much less significant for charged laser-heated films.

Figure 12 exhibits the evolution of the absorption α and the scattered intensity w_1 with increasing A, that is, with decreasing film thickness or increasing film temperature (i.e., increasing Debye length). For a charged ($\eta=0.1$) hot laser-heated film with $\gamma=10^{-3}$ and $\tilde{\sigma}=10^{-2}$, we show results for (a) $A=10^{-4}$, (b) 10^{-3}, (c) 3×10^{-3}, and (d) 10^{-2}. Again, as in the case of a neutral film, the plasma resonance broadens with increasing A and ultimately disappears for $A=10^{-2}$. These results demonstrate once again that for a correct description of the plasma resonance in laser-excited-driven nano-objects, the effects of Landau damping related to its finite size must be taken into account and that this effect is present already in the hydrodynamic approximation.

B. Second-order and third-order approximations

To calculate the third-harmonic response, we must solve the perturbation-theory equations both to second and to third orders. For $A\neq0$, the corresponding formulas are very cumbersome, and they have been delegated to the Appendix. The final equations are Eqs. (A5a) and (A5b) for cold metal films and hot laser-heated films, respectively. In the former case, Eq. (A5a) must be solved with the boundary conditions $\tilde{q}_2[\pm(1+\tilde{\sigma})/(2\sqrt{A})]=0$ and $\tilde{q}_3[\pm(1+\tilde{\sigma})/(2\sqrt{A})]=0$, corresponding to the vanishing electron current everywhere outside the film. In order to be consistent with the case of $A=0$ [see Eq. (30)], the dipole-moment amplitude d_3 at the triple laser frequency should be defined as

$$d_3=-\frac{1}{\sqrt{A}}\int_{-(1+\tilde{\sigma})/(2\sqrt{A})}^{(1+\tilde{\sigma})/(2\sqrt{A})}\tilde{n}_3(\tilde{\zeta})\tilde{\zeta}d\tilde{\zeta}=-\frac{1}{\sqrt{A}}\int_{-(1+\tilde{\sigma})/(2\sqrt{A})}^{(1+\tilde{\sigma})/(2\sqrt{A})}i\tilde{q}_3(\tilde{\zeta})d\tilde{\zeta},$$

with the same definition as before for the reduced third-harmonic intensity $\tilde{w}_3$. For hot and charged laser-heated films, the boundary conditions to Eq. (A5b) should be $\tilde{q}_2(\pm\infty)=0$ and $\tilde{q}_3(\pm\infty)=0$ as above, due to the Debye tailing. Correspondingly, the dipole-moment amplitude should be defined as $d_3=-A^{-1/2}\int_{-\infty}^{\infty}i\tilde{q}_3(\tilde{\zeta})d\tilde{\zeta}$. Results calculated for the third-order harmonic intensity $\tilde{w}_3$ are presented and discussed in Secs. IV B 1 and IV B 2 for cold metal films and hot laser-ionized films, respectively.

1. Cold metal films

The results of the calculations of the third-harmonic intensity as a function of laser frequency are presented in Figs. 13 and 14 for two different values of the parameter A. Figure 13 shows the frequency dependence of the third-harmonic intensity $\tilde{w}_3$ for a neutral cold metal film with $A=10^{-7}$, $\gamma=10^{-3}$, and with $\tilde{\sigma}$ equal to (a) 1.5×10^{-3}, (b) 3×10^{-3}, (c) 6×10^{-3}, and (d) 10^{-2}. Disregarding details, the third-harmonic intensity $\tilde{w}_3$ in the case of small reduced film-boundary thickness $\tilde{\sigma}=1.5\times10^{-3}$ [Fig. 13(a)] exhibits four resonant peaks grouped in two pairs, which correspond to laser frequencies approximately equal to the plasma frequency and to one third of it. As compared with the corresponding Fig. 7(a) with the same parameters for the linear case, a one-to-one correspondence is observed between the two closely spaced peaks near the plasma frequency in linear absorption in Fig. 7(a) and in the third-harmonic intensity in Fig. 13(a). For the third harmonic, the pattern of two closely spaced resonant peaks is repeated near one third of the

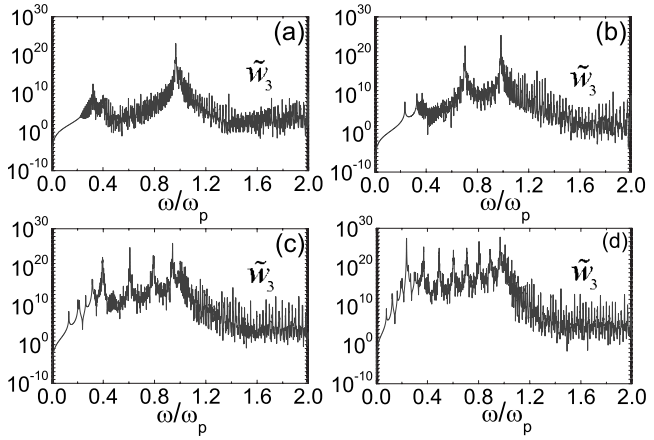

FIG. 14. Frequency dependence of the third-harmonic intensity $\tilde{w}_3$ for a neutral cold metal film with $A=10^{-5}$, $\gamma=10^{-3}$, and with $\tilde{\sigma}$ equal to (a) 1.5×10^{-2}, (b) 3×10^{-2}, (c) 6×10^{-2}, and (d) 10^{-1}.

plasma frequency. Of course, there is no corresponding feature in linear absorption. Yet another difference between the linear absorption of Fig. 7(a) and the third-harmonic intensity of Fig. 13(a) is that from the two closely spaced peaks near the plasma frequency, the right peak, which corresponds to the bulk-plasma resonance at $\tilde{\omega}=1$, is dominant for linear absorption, while this is not the case for the third-harmonic intensity. In the latter case, the left peak, which appears due to the increasing film-boundary thickness, is dominant. This can be naturally explained by the dominant role of the film boundary in the formation of the third-order response of the film, while the bulk here plays only a minor role. With increasing $\tilde{\sigma}$, the resonance peaks in the third-harmonic intensity continue to appear in two groups, one in the same position as the corresponding additional peaks in the linear absorption (cf. Fig. 13 with Fig. 7 for the same conditions), while the second group is located near and below one third of the linear-absorption resonance frequency. As was the case for linear absorption, the number of peaks increases with increasing $\tilde{\sigma}$. All this suggests that the third-harmonic resonances and the linear-absorption resonances are closely related.

The magnitude of the third-harmonic yield can again be estimated from Eq. (31), as was done at the end of Sec. III for the case of $A=0$. A film with thickness of $a=100$ nm and boundary thickness of $\sigma=0.6$ nm corresponds to the case of Fig. 13(c) (with $\tilde{\sigma}=6\times10^{-3}$). If again we assume $n_i z_{\text{ion}}=2\times10^{22}$ cm^{-3} (with $\lambda_p=242$ nm) and the laser operating at the wavelength $\lambda\approx3\lambda_p$ with intensity $I_0=10^{10}$ W/cm^2, we obtain from Eq. (31) a conversion efficiency of $\sigma_{\text{scatt}(3\omega)}/S_L\approx2.7\times10^{-13}\tilde{w}_3$. With the results of Fig. 13(c), this means that the conversion efficiency to the third harmonic over a wide range of frequencies near the third-order resonance is of the order of 10^{-3} and substantially higher very close to the resonances. As a general trend, Fig. 13 indicates that the background value of the third-harmonic yield increases with increasing $\tilde{\sigma}$, in the case of moderate incident laser intensities that satisfy the perturbation-theory condition for $A\neq0$.

The correspondence between the extra linear-absorption resonances and the third-harmonic resonances remains the same for other values of A. Figure 14 shows the frequency dependence of the third-harmonic intensity $\tilde{w}_3$ for a neutral cold metal film with $A=10^{-5}$, $\gamma=10^{-3}$, and with $\tilde{\sigma}$ equal to (a) 1.5×10^{-2}, (b) 3×10^{-2}, (c) 6×10^{-2}, and (d) 10^{-1}, which like before can be compared with the linear-absorption resonances exhibited in Fig. 8 under the same conditions. However, the calculated third-harmonic intensity curve is much noisier than in the previous case of $A=10^{-7}$. This noise increases with increasing A (with decreasing film thickness). We checked that for the artificially small value of $A=10^{-9}$ (for rather thick film in our conditions), the corresponding third-harmonic intensity curve is completely noise free. At the time of this writing, it was not clear whether this noise has a physical origin or is a numerical artifact.

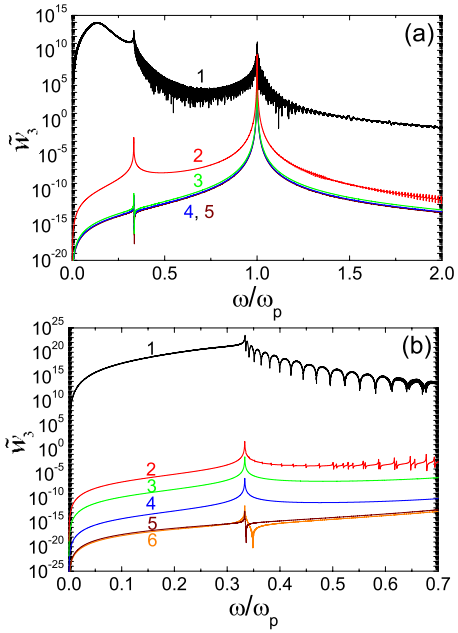

FIG. 15. (Color online) Frequency dependence of the third-harmonic intensity $\tilde{w}_3$ for a hot laser-ionized film. Panel (a): $A=10^{-5}$, $\gamma=10^{-3}$, $\tilde{\sigma}=10^{-2}$, and the curves from 1 to 5 correspond to outer-ionization degrees $\eta=0$, 0.03, 0.05, 0.1, and 0.15, respectively. Panel (b) shows a restricted frequency range only in the vicinity of the third-order resonance for $A=10^{-4}$, $\gamma=10^{-3}$, and $\tilde{\sigma}=10^{-2}$. The curves from 1 to 6 correspond to outer-ionization degrees $\eta=0$, 0.05, 0.075, 0.1, 0.15, and 0.2, respectively.

2. Laser-heated/ionized films

In contrast to cold metal nanofilms, only one classical third-order resonance at one third of the bulk-plasma resonance frequency appears in the frequency dependence of the third-harmonic intensity in the case when the nanofilm is laser heated/ionized. Results of calculations for this case for different values of the outer-ionization degree are presented in panels (a) and (b) of Fig. 15 for the two values $A=10^{-5}$ and 10^{-4} [in panel (b), only the frequency range of interest near the third-order resonance is shown]. For a laser-heated film, the existence of only one classical third-order resonance is to be expected because there are no extra resonances in the corresponding linear response of the film, at least below the nominal plasma resonance frequency. More importantly, the

third-harmonic intensity extremely strongly depends on the outer-ionization degree η, at least for the small η values below some critical value. Namely, the third-harmonic intensity drops extremely fast with increasing η with respect to the case of a neutral film with $\eta=0$. Apparently, this is a consequence of the decreasing electron density in the film-boundary range with increasing η. Then, upon a further increase in η, the third-harmonic intensity saturates at a very low level. For $A=10^{-5}$ [Fig. 15(a)], the third-harmonic intensity is almost saturated already at $\eta=0.05$, while for $A=10^{-4}$ [Fig. 15(b)] saturation of the third-harmonic intensity occurs at the higher value of $\eta=0.15$. For such high values of the outer-ionization degree the film-boundary range is almost completely depleted of electrons (cf. Fig. 3 for the quasiequilibrium regime) and the bulk range of the film begins to play the decisive role in the formation of the third-harmonic response. Besides, it should be noted that the form of the third-order resonance curve in the vicinity of the resonance is quite different before and after the onset of saturation. This indicates that the mechanism of the third-harmonic generation is different in these two ranges of the outer-ionization degree.

V. CONCLUSIONS

In this paper, both the linear and the third-order nonlinear electron responses of a thin free-electron nanofilm with diffuse boundaries to the action of linearly p-polarized laser light were considered in the hydrodynamic approximation. The third-order nonlinear response including generation of the third harmonic of the driving laser was investigated. The nonlinearity is introduced through the basic nonlinearity of the current-field interaction and the convective derivative in the equation of motion. A corresponding nonlinearity exists in the hydrodynamic equation for the electron pressure. The effect of the nonlinearities is especially pronounced in the film boundaries owing to the corresponding short-scale variation in the electron density, the effective electric field, and the electron velocity. According to our model, third-harmonic generation can be very substantial (with an average efficiency of the order 10^{-3} and still higher near resonances). It is entirely confined to the film boundaries. Like for the linear response, it may be resonantly enhanced below the bulk-plasma resonance frequency. Both cold metal nanofilms and hot laser-heated and/or ionized nanofilms are analyzed in detail in the framework of the same approach. For a hot film, its possible outer ionization by the laser prepulse essentially influences the third-harmonic yield due to the reduced electron density in the boundary range of the film as compared with the corresponding neutral film.

In order to use analytical methods as far as possible in this very stiff problem (from the numerical point of view), the stationary approximation as well as perturbation theory were used. In addition, the ions were considered frozen. This allowed us to limit the study of the response to the electron subsystem of the nanofilm and to investigate the laser frequency dependence of the linear absorption and the third-harmonic intensity and also to evaluate both the linear and the nonlinear excitations of the plasma resonance. It turns out that, at least in a neutral cold metal nanofilm, both of these phenomena strongly depend on the film-boundary diffuseness (that is, the boundary thickness) if they are not completely determined by the film edges. Two different perturbation theories were distinguished in this context. One of them works only for neutral films and corresponds to sufficiently high laser fields with amplitude E_0 in the range of $E_l \ll E_0 \ll E_\sigma$, while the other one is applicable both for neutral and for laser-ionized (locally charged) films and corresponds to lower laser fields $E_0 \ll E_l$. Here, E_l and E_σ denote the reference electric fields that are connected, respectively, either with the spatial charge separation length (l_Q or l_D for cold or hot nanofilms) or with the thickness σ of the diffuse boundary.

It was shown that in the frequency range below the bulk-plasma resonance, the linear absorption in a thin nanofilm with diffuse boundaries can be much higher than for a similar film with sharp (stepwise) edges. For cold neutral metal nanofilms and moderate laser fields, it was found that the frequency dependence of the linear absorption consists of extra quasiequally spaced resonance peaks below the nominal plasma resonance peak. (Note that the experimentally measured optical absorption of a thin silicon film of 2.33 μm thickness, which was exhibited as an example in Ref. 46, demonstrates a similar oscillatory behavior as a function of the photon energy.) In our model the number of such absorption peaks increases with increasing film-boundary thickness, and the extra absorption in this frequency range is completely determined by the film boundaries. These resonances become even more pronounced in the third-order response, where they generate an additional nonlinear resonance sequence at frequencies of one third of the parent resonance frequencies. In contrast, for hot laser-heated films the extra resonances both in the linear absorption and in the third-harmonic response do not appear. Apart from some global increase in the linear absorption in the low-frequency range, only the nominal plasma resonance and its nonlinear third-order offspring at one third of the resonance frequency appear in the corresponding frequency spectra. On the other hand, the influence of the full film thickness (i.e., of the parameter A) and especially of the outer-ionization degree on the resonance profile of both the linear absorption and the third-order nonlinear response is significant. The latter is also tightly connected with the film-boundary effect due to the strong dependence of the nonuniform electron density in the boundary range on the outer-ionization degree.

Though most recent experimental studies have been carried out with short-pulse laser beams, we hope that the results obtained in this paper may be useful, if not for direct comparison with the experimental data obtained for short laser pulses, then for the deeper understanding of the mechanisms of the interaction of laser light with nanofilms, as well as with other nano-objects such as nanoclusters, taking into account the boundary effects. Regarding experiments on the interaction of lasers with nanofilms, especially on laser absorption and third-harmonic generation, the parameters most relevant to our work are the laser frequency and polarization, and the film thickness and the film-boundary thickness. It is not very clear at the moment whether or not it is possible to

control experimentally the thickness of the diffuse film boundary, even though this parameter is crucial for our study. Maybe this will become feasible in the future due to the rapid progress of nanophysics and nanotechnologies. But the other three parameters may be well controlled already now. In this context, one should distinguish the volume and the surface contributions to laser absorption and third-harmonic generation in thin nanofilms with free electrons (note that bound electrons can also contribute to the corresponding volume contributions). Our work is primarily concerned with the collisionless (with respect to binary collisions) surface contributions of free electrons in the restricted geometry of the thin films.

First, both linear and nonlinear effects strongly depend on the polarization of the incident wave. The collisionless contributions should vanish for the case of *s*-polarized laser light where only the volume contributions are important. In contrast, for obliquely incident *p*-polarized laser light and thin nanofilms, the collisionless contributions may dominate. In this case, in particular, it may occur that third-harmonic radiation will only be observed for laser light with oblique *p* polarization. The volume contribution and the collisionless surface contribution depend differently on the film thickness a and the boundary thickness σ (if the other parameters are kept constant). Ignoring for simplicity frequencies near the resonances for $A \neq 0$, one may conclude that the collisional contribution (associated with the small relaxation constant γ) to the absorption cross section [Eq. (20)] depends linearly on a, while the collisionless contribution is independent of a but depends linearly on the film-boundary thickness σ [cf. the two contributions to α in Eqs. (21) and (22) for the benchmark case of $A=0$]. This confirms the identification of the former with the volume contribution and the latter with the surface term.

We can make the same distinction for the scattering cross section [Eq. (29)] into the third harmonic. Again for the case of $A=0$, the collisionless contribution is proportional to $1/\sigma^2$ [since $w_3 \sim (a/\sigma)^2$], and it only appears in our model (in spite of including the relaxation constant γ) because the only physical source of the third-order nonlinearity is the density gradient in the diffusive boundaries of the film. Note that the collisionless contribution to the third-harmonic cross section $\sigma_{\mathrm{scat}(3\omega)}$ is again independent of a as should be the case for the surface contribution. It will be dominant for sufficiently small film-boundary thickness σ, in contrast to the case of linear absorption. The volume contribution to the third-harmonic radiation, which does not appear in our model but may arise, e.g., at least from bound electrons, should be proportional to a^2. (The above scaling for the third-harmonic contributions is valid for $a \ll \lambda$ and $l \ll \sigma \ll a$, where $l=l_Q$ or $l=l_D$.) The two different contributions (surface and volume) to linear laser absorption and third-harmonic generation could be distinguished experimentally by their different dependence on a and σ, at least for cold metal nanofilms. Finally, the collisionless (surface) and the volume contributions can be distinguished by their different frequency dependence, especially for cold metal nanofilms at moderate laser intensity ($E_0 \ll E_l$). In the latter case, the specific resonance structure below the bulk-plasma frequency should manifest itself if the collisionless surface contributions are those that are dominant. The effect of increasing laser absorption by the film with increasing film-boundary thickness may find important applications if control of the thickness of the diffuse film boundaries will become experimentally possible.

The effects discussed in this paper may be important not only for long laser pulses, for which the stationary approximation is definitely applicable, but also for short pulses. Going beyond the stationary approximation as well as perturbation theory and performing completely numerical simulations for realistic conditions of the laser-film interaction may be the subject of future work.

ACKNOWLEDGMENTS

The authors are grateful to Sergey V. Popruzhenko for fruitful discussions. This work was supported by the Deutsche Forschungsgemeinschaft [Project No. 436 RUS 113/852/0-1(R)] and by the Russian Foundation for Basic Research (Grants No. 06-02-04006NNIO-a and No. 06-02-16916).

APPENDIX: EQUATIONS FOR THE AMPLITUDES OF THE SECOND AND THIRD ORDERS ($A \neq 0$)

When applying the perturbation series of Eq. (33) to the complete nonlinear system of Eqs. (32a)–(32c), in the second-order approximation, Eqs. (32b) and (32c) for the electron current and pressure amplitudes, respectively, result in the equations

$$n_0^2\left(-2i+\frac{\gamma}{\tilde{\omega}}\right)\tilde{q}_2+n_0\tilde{n}_1\left(-i+\frac{\gamma}{\tilde{\omega}}\right)\tilde{q}_1+n_0\tilde{q}_1\frac{d\tilde{q}_1}{d\tilde{\zeta}}-\frac{\tilde{q}_1^2}{2}\frac{dn_0}{d\tilde{\zeta}}+\frac{1}{\tilde{\omega}^2}\left\{n_0^2\frac{dP_2}{d\tilde{\zeta}}+n_0\tilde{n}_1\frac{dP_1}{d\tilde{\zeta}}+2n_0\tilde{n}_2\frac{dP_0}{d\tilde{\zeta}}+\frac{\tilde{n}_1^2}{2}\frac{dP_0}{d\tilde{\zeta}}+n_0^3\tilde{f}_2+\frac{3\tilde{n}_1n_0^2(1+\tilde{f}_1)}{2}+3\tilde{n}_2n_0^2\tilde{f}_0+\frac{3\tilde{n}_1^2n_0\tilde{f}_0}{2}\right\}=0, \tag{A1a}$$

$$-2in_0^2P_2-in_0\tilde{n}_1P_1+\tilde{q}_2n_0\frac{dP_0}{d\tilde{\zeta}}+\frac{\tilde{q}_1}{2}\left(n_0\frac{dP_1}{d\tilde{\zeta}}+\tilde{n}_1\frac{dP_0}{d\tilde{\zeta}}\right)+3P_0n_0\frac{d\tilde{q}_2}{d\tilde{\zeta}}+\frac{3(P_0\tilde{n}_1+n_0P_1)}{2}\frac{d\tilde{q}_1}{d\tilde{\zeta}}-3\tilde{q}_2P_0\frac{dn_0}{d\tilde{\zeta}}-\frac{3\tilde{q}_1}{2}\left(P_1\frac{dn_0}{d\tilde{\zeta}}+P_0\frac{d\tilde{n}_1}{d\tilde{\zeta}}\right)=0. \tag{A1b}$$

These equations, together with the corresponding Eq. (34) can be reduced to a single equation for the second-order electron current amplitude $\tilde{q}_2(\tilde{\zeta})$,

$$\frac{3P_0}{2n_0}\frac{d^2(i\tilde{q}_2)}{d\tilde{\zeta}^2}+\frac{d(i\tilde{q}_2)}{d\tilde{\zeta}}\left\{-\frac{3\tilde{f}_0}{2}-\frac{3P_0}{n_0^2}\frac{dn_0}{d\tilde{\zeta}}\right\}+i\tilde{q}_2\left\{\frac{d}{d\tilde{\zeta}}\left(-\frac{\tilde{f}_0}{2}-\frac{3P_0}{2n_0^2}\frac{dn_0}{d\tilde{\zeta}}\right)-\frac{n_0}{2}+2\tilde{\omega}^2+i\gamma\tilde{\omega}\right\}-\frac{\tilde{n}_1}{n_0}\frac{dP_1}{d\tilde{\zeta}}-\frac{\tilde{n}_1^2}{2n_0^2}\frac{dP_0}{d\tilde{\zeta}}$$
$$-\frac{3\tilde{n}_1(1+\tilde{f}_1)}{2}-\frac{3\tilde{n}_1^2\tilde{f}_0}{2n_0}+\frac{\tilde{n}_1(\tilde{\omega}^2+i\gamma\tilde{\omega})i\tilde{q}_1}{n_0}+\tilde{\omega}^2\left\{\frac{i\tilde{q}_1}{n_0}\frac{d(i\tilde{q}_1)}{d\tilde{\zeta}}-\frac{(i\tilde{q}_1)^2}{2n_0^2}\frac{dn_0}{d\tilde{\zeta}}\right\}+\frac{d}{d\tilde{\zeta}}\left\{\frac{\tilde{n}_1P_1}{2n_0}+\frac{i\tilde{q}_1}{4n_0^2}\left(n_0\frac{dP_1}{d\tilde{\zeta}}+\tilde{n}_1\frac{dP_0}{d\tilde{\zeta}}\right)\right.$$
$$\left.+\frac{3(P_0\tilde{n}_1+n_0P_1)}{4n_0^2}\frac{d(i\tilde{q}_1)}{d\tilde{\zeta}}-\frac{3(i\tilde{q}_1)}{4n_0^2}\left(P_1\frac{dn_0}{d\tilde{\zeta}}+P_0\frac{d\tilde{n}_1}{d\tilde{\zeta}}\right)\right\}=0. \tag{A2}$$

Similarly, the equations for the electron current and pressure amplitudes of the third-order approximation can be obtained as follows:

$$n_0^2\left(-3i+\frac{\gamma}{\tilde{\omega}}\right)\tilde{q}_3+n_0\tilde{n}_1\left(-2i+\frac{\gamma}{\tilde{\omega}}\right)\tilde{q}_2+\left(n_0\tilde{n}_2+\frac{\tilde{n}_1^2}{4}\right)\left(-i+\frac{\gamma}{\tilde{\omega}}\right)\tilde{q}_1+n_0\tilde{q}_1\frac{d\tilde{q}_2}{d\tilde{\zeta}}+n_0\tilde{q}_2\frac{d\tilde{q}_1}{d\tilde{\zeta}}+\frac{\tilde{n}_1\tilde{q}_1}{2}\frac{d\tilde{q}_1}{d\tilde{\zeta}}-\frac{\tilde{q}_1^2}{4}\frac{d\tilde{n}_1}{d\tilde{\zeta}}-\tilde{q}_1\tilde{q}_2\frac{dn_0}{d\tilde{\zeta}}$$
$$+\frac{1}{\tilde{\omega}^2}\left\{n_0^2\frac{dP_3}{d\tilde{\zeta}}+n_0\tilde{n}_1\frac{dP_2}{d\tilde{\zeta}}+n_0\tilde{n}_2\frac{dP_1}{d\tilde{\zeta}}+\frac{\tilde{n}_1^2}{4}\frac{dP_1}{d\tilde{\zeta}}+2n_0\tilde{n}_3\frac{dP_0}{d\tilde{\zeta}}+\tilde{n}_1\tilde{n}_2\frac{dP_0}{d\tilde{\zeta}}+n_0^3\tilde{f}_3+\frac{3\tilde{n}_1n_0^2\tilde{f}_2}{2}+\left(\frac{3\tilde{n}_2n_0^2}{2}+\frac{3\tilde{n}_1^2n_0}{4}\right)(1+\tilde{f}_1)\right.$$
$$\left.+3\tilde{n}_3n_0^2\tilde{f}_0+\frac{\tilde{n}_1^3\tilde{f}_0}{4}+3n_0\tilde{n}_1\tilde{n}_2\tilde{f}_0\right\}=0, \tag{A3a}$$

$$-3in_0^2P_3-2in_0\tilde{n}_1P_2-in_0\tilde{n}_2P_1-\frac{i\tilde{n}_1^2P_1}{4}+\tilde{q}_3n_0\frac{dP_0}{d\tilde{\zeta}}+\frac{\tilde{q}_2}{2}\left(n_0\frac{dP_1}{d\tilde{\zeta}}+\tilde{n}_1\frac{dP_0}{d\tilde{\zeta}}\right)+\frac{\tilde{q}_1}{2}\left(n_0\frac{dP_2}{d\tilde{\zeta}}+\tilde{n}_2\frac{dP_0}{d\tilde{\zeta}}+\frac{\tilde{n}_1}{2}\frac{dP_1}{d\tilde{\zeta}}\right)$$
$$+3P_0n_0\frac{d\tilde{q}_3}{d\tilde{\zeta}}+\frac{3(P_0\tilde{n}_1+n_0P_1)}{2}\frac{d\tilde{q}_2}{d\tilde{\zeta}}+\frac{3}{2}\left(P_0\tilde{n}_2+n_0P_2+\frac{\tilde{n}_1P_1}{2}\right)\frac{d\tilde{q}_1}{d\tilde{\zeta}}-3\tilde{q}_3P_0\frac{dn_0}{d\tilde{\zeta}}$$
$$-\frac{3\tilde{q}_2}{2}\left(P_1\frac{dn_0}{d\tilde{\zeta}}+P_0\frac{d\tilde{n}_1}{d\tilde{\zeta}}\right)-\frac{3\tilde{q}_1}{2}\left(P_2\frac{dn_0}{d\tilde{\zeta}}+P_0\frac{d\tilde{n}_2}{d\tilde{\zeta}}+\frac{P_1}{2}\frac{d\tilde{n}_1}{d\tilde{\zeta}}\right)=0. \tag{A3b}$$

Again, Eqs. (A3a) and (A3b) can be reduced to a single equation for the third-order electron current amplitude $\tilde{q}_3(\tilde{\zeta})$,

$$\frac{P_0}{n_0}\frac{d^2(i\tilde{q}_3)}{d\tilde{\zeta}^2}+\frac{d(i\tilde{q}_3)}{d\tilde{\zeta}}\left\{-\tilde{f}_0-\frac{2P_0}{n_0^2}\frac{dn_0}{d\tilde{\zeta}}\right\}+i\tilde{q}_3\left\{\frac{d}{d\tilde{\zeta}}\left(-\frac{\tilde{f}_0}{3}-\frac{P_0}{n_0^2}\frac{dn_0}{d\tilde{\zeta}}\right)-\frac{n_0}{3}+3\tilde{\omega}^2+i\gamma\tilde{\omega}\right\}-\frac{\tilde{n}_1}{n_0}\frac{dP_2}{d\tilde{\zeta}}-\frac{\tilde{n}_2}{n_0}\frac{dP_1}{d\tilde{\zeta}}-\frac{\tilde{n}_1^2}{4n_0^2}\frac{dP_1}{d\tilde{\zeta}}-\frac{\tilde{n}_1\tilde{n}_2}{n_0^2}\frac{dP_0}{d\tilde{\zeta}}$$
$$-\frac{3\tilde{n}_1\tilde{f}_2}{2}-\left(\frac{3\tilde{n}_2}{2}+\frac{3\tilde{n}_1^2}{4n_0}\right)(1+\tilde{f}_1)-\frac{\tilde{n}_1^3\tilde{f}_0}{4n_0^2}-\frac{3\tilde{n}_1\tilde{n}_2\tilde{f}_0}{n_0}-\tilde{\omega}^2\left\{\frac{(i\tilde{q}_1)(i\tilde{q}_2)}{n_0^2}\frac{dn_0}{d\tilde{\zeta}}+\frac{(i\tilde{q}_1)^2}{4n_0^2}\frac{d\tilde{n}_1}{d\tilde{\zeta}}\right\}$$
$$+\tilde{\omega}^2\left\{\frac{(i\tilde{q}_1)\tilde{n}_1}{2n_0^2}\frac{d(i\tilde{q}_1)}{d\tilde{\zeta}}+\frac{i\tilde{q}_2}{n_0}\frac{d(i\tilde{q}_1)}{d\tilde{\zeta}}+\frac{i\tilde{q}_1}{n_0}\frac{d(i\tilde{q}_2)}{d\tilde{\zeta}}\right\}+\left(\frac{\tilde{n}_1^2}{4n_0^2}+\frac{\tilde{n}_2}{n_0}\right)(\tilde{\omega}^2+i\gamma\tilde{\omega})i\tilde{q}_1+\frac{\tilde{n}_1(2\tilde{\omega}^2+i\gamma\tilde{\omega})i\tilde{q}_2}{n_0}$$
$$+\frac{d}{d\tilde{\zeta}}\left(\frac{2\tilde{n}_1P_2}{3n_0}+\frac{\tilde{n}_2P_1}{3n_0}+\frac{\tilde{n}_1^2P_1}{12n_0^2}\right)+\frac{d}{d\tilde{\zeta}}\left\{\frac{i\tilde{q}_2}{6n_0^2}\left(n_0\frac{dP_1}{d\tilde{\zeta}}+\tilde{n}_1\frac{dP_0}{d\tilde{\zeta}}\right)+\frac{i\tilde{q}_1}{6n_0^2}\left(n_0\frac{dP_2}{d\tilde{\zeta}}+\tilde{n}_2\frac{dP_0}{d\tilde{\zeta}}+\frac{\tilde{n}_1}{2}\frac{dP_1}{d\tilde{\zeta}}\right)+\frac{(P_0\tilde{n}_1+n_0P_1)}{2n_0^2}\frac{d(i\tilde{q}_2)}{d\tilde{\zeta}}\right\}$$
$$+\frac{d}{d\tilde{\zeta}}\left\{\frac{1}{2n_0^2}\frac{d(i\tilde{q}_1)}{d\tilde{\zeta}}\left(P_0\tilde{n}_2+n_0P_2+\frac{\tilde{n}_1P_1}{2}\right)-\frac{i\tilde{q}_2}{2n_0^2}\left(P_1\frac{dn_0}{d\tilde{\zeta}}+P_0\frac{d\tilde{n}_1}{d\tilde{\zeta}}\right)-\frac{i\tilde{q}_1}{2n_0^2}\left(P_2\frac{dn_0}{d\tilde{\zeta}}+P_0\frac{d\tilde{n}_2}{d\tilde{\zeta}}+\frac{P_1}{2}\frac{d\tilde{n}_1}{d\tilde{\zeta}}\right)\right\}=0. \tag{A4}$$

Equations (A2) and (A4) can be simplified in the cases of cold metal films with $P_0=n_0^{5/3}$ and hot laser-heated films with $P_0=n_0$ as follows. The first-order amplitudes that occur in Eqs. (A2) and (A4) can be eliminated with the help of the first-order Eq. (35), while the second-order amplitudes occurring in Eq. (A4) can be eliminated with the help of the second-order Eqs. (A1a) and (A1b). In these two cases of cold metal films (CF) and hot laser-heated films (HF), the final equations can be written in a compact form, respectively, as the following Eqs. (A5a) and (A5b), with $k=2$ for the second-order equations and $k=3$ for the third-order equations:

$$\frac{3n_0^{2/3}}{k}\frac{d^2(i\tilde{q}_k)}{d\tilde{\zeta}^2}+\frac{3\tilde{f}_0}{5k}\frac{d(i\tilde{q}_k)}{d\tilde{\zeta}}+i\tilde{q}_k\left(\frac{4}{5k}\frac{d\tilde{f}_0}{d\tilde{\zeta}}-\frac{n_0}{k}+k\tilde{\omega}^2+i\gamma\tilde{\omega}\right)+T_k^{\mathrm{CF}}=0, \tag{A5a}$$

$$\frac{3}{k}\frac{d^2(i\tilde{q}_k)}{d\tilde{\zeta}^2}+\frac{3\tilde{f}_0}{k}\frac{d(i\tilde{q}_k)}{d\tilde{\zeta}}+i\tilde{q}_k\left(\frac{2}{k}\frac{d\tilde{f}_0}{d\tilde{\zeta}}-\frac{n_0}{k}+k\tilde{\omega}^2+i\gamma\tilde{\omega}\right)+T_k^{\mathrm{HF}}=0. \tag{A5b}$$

Moreover, substituting $k=1$ in Eqs. (A5a) and (A5b) we retrieve the linear-approximation Eqs. (37a) and (37b) with the first-order free terms $T_1^{\mathrm{CF}}=T_1^{\mathrm{HF}}=-n_0$. The corresponding second-order free terms T_2^{CF} and T_2^{HF} are

$$T_2^{\mathrm{CF}}=\frac{\tilde{n}_1(1+i\tilde{q}_1)}{2}-\frac{\tilde{n}_1 i\tilde{q}_1(2\tilde{\omega}^2+i\gamma\tilde{\omega})}{n_0}-\frac{9\tilde{n}_1^2\tilde{f}_0}{10n_0}+\frac{4i\tilde{q}_1\tilde{n}_1\tilde{f}_0'}{5n_0}-\frac{(i\tilde{q}_1)^2\tilde{f}_0''}{5n_0}$$
$$-\frac{i\tilde{q}_1\tilde{f}_0\{20n_0+5i\tilde{q}_1(4n_0-7\tilde{\omega}^2-4i\gamma\tilde{\omega})-60\tilde{f}_0\tilde{n}_1+26i\tilde{q}_1\tilde{f}_0'\}}{50n_0^{5/3}}-\frac{9(i\tilde{q}_1)^2\tilde{f}_0^3}{25n_0^{7/3}}, \tag{A6a}$$

$$T_2^{\mathrm{HF}}=\frac{\tilde{n}_1(1+i\tilde{q}_1)}{2}-\frac{\tilde{n}_1 i\tilde{q}_1(2\tilde{\omega}^2+i\gamma\tilde{\omega})}{n_0}-\frac{3\tilde{n}_1^2\tilde{f}_0}{2n_0}+\frac{2i\tilde{q}_1\tilde{n}_1\tilde{f}_0'}{n_0}-\frac{(i\tilde{q}_1)^2\tilde{f}_0''}{2n_0}$$
$$-\frac{i\tilde{q}_1\tilde{f}_0\{2n_0+i\tilde{q}_1(2n_0-3\tilde{\omega}^2-2i\gamma\tilde{\omega})-6\tilde{f}_0\tilde{n}_1+3i\tilde{q}_1\tilde{f}_0'\}}{2n_0}-\frac{3(i\tilde{q}_1)^2\tilde{f}_0^3}{2n_0}, \tag{A6b}$$

while the third-order free terms T_3^{CF} and T_3^{HF} are obtained as the following rather cumbersome expressions, in which all of the individual terms are the terms of the same order and can only be distinguished by their different $\tilde{\zeta}$ dependence,

$$T_3^{\mathrm{CF}}=\frac{\tilde{n}_1 i\tilde{q}_2}{4}+\frac{\tilde{n}_2(1+i\tilde{q}_1)}{2}-\frac{\tilde{n}_1^2(1+i\tilde{q}_1)}{4n_0}-\frac{(i\tilde{q}_1\tilde{n}_2+i\tilde{q}_2\tilde{n}_1)(3\tilde{\omega}^2+i\gamma\tilde{\omega})}{n_0}+\frac{3i\tilde{q}_1\tilde{n}_1^2(3\tilde{\omega}^2+i\gamma\tilde{\omega})}{4n_0^2}+\frac{\tilde{n}_1^3\tilde{f}_0}{4n_0^2}-\frac{9\tilde{n}_1\tilde{n}_2\tilde{f}_0}{5n_0}+\frac{2\tilde{n}_1 i\tilde{q}_2\tilde{f}_0'}{5n_0}$$
$$+\frac{4\tilde{n}_2 i\tilde{q}_1\tilde{f}_0'}{5n_0}+\frac{\tilde{n}_1^2 i\tilde{q}_1\tilde{f}_0'}{5n_0^2}-\frac{i\tilde{q}_1 i\tilde{q}_2\tilde{f}_0''}{5n_0}-\frac{(i\tilde{q}_1)^2\tilde{n}_1\tilde{f}_0''}{5n_0^2}+\frac{(i\tilde{q}_1)^3\tilde{f}_0'''}{30n_0^2}+\frac{\tilde{\omega}^2(i\tilde{q}_1)^2\{n_0+i\tilde{q}_1(n_0-\tilde{\omega}^2-i\gamma\tilde{\omega})\}}{12n_0^{8/3}}$$
$$+\frac{(i\tilde{q}_1)^2\tilde{n}_1\tilde{f}_0(4n_0-27\tilde{\omega}^2-8i\gamma\tilde{\omega})}{20n_0^{8/3}}+\frac{(i\tilde{q}_1\tilde{n}_1-i\tilde{q}_2n_0)\tilde{f}_0}{5n_0^{5/3}}+\frac{i\tilde{q}_1 i\tilde{q}_2\tilde{f}_0(8\tilde{\omega}^2+3i\gamma\tilde{\omega}-2n_0)}{5n_0^{5/3}}+\frac{3(i\tilde{q}_2\tilde{n}_1+2i\tilde{q}_1\tilde{n}_2)\tilde{f}_0^2}{5n_0^{5/3}}$$
$$+\frac{(i\tilde{q}_1)^2(1+i\tilde{q}_1)\tilde{f}_0'}{10n_0^{5/3}}+\frac{3(i\tilde{q}_1)^3\tilde{f}_0'^2}{25n_0^{8/3}}-\frac{(i\tilde{q}_1)^3\tilde{f}_0'(5\tilde{\omega}^2+3i\gamma\tilde{\omega})}{30n_0^{8/3}}-\frac{41(i\tilde{q}_1)^2\tilde{n}_1\tilde{f}_0\tilde{f}_0'}{50n_0^{8/3}}-\frac{13i\tilde{q}_1 i\tilde{q}_2\tilde{f}_0\tilde{f}_0'}{25n_0^{5/3}}+\frac{4(i\tilde{q}_1)^3\tilde{f}_0\tilde{f}_0''}{25n_0^{8/3}}+\frac{24(i\tilde{q}_1)^3\tilde{f}_0^4}{125n_0^4}$$
$$+\frac{i\tilde{q}_1\tilde{f}_0^2\{5i\tilde{q}_1n_0+5(i\tilde{q}_1)^2(n_0+5\tilde{\omega}^2-i\gamma\tilde{\omega})-90n_0i\tilde{q}_2\tilde{f}_0-105i\tilde{q}_1\tilde{n}_1\tilde{f}_0+118(i\tilde{q}_1)^2\tilde{f}_0'\}}{250n_0^{10/3}}, \tag{A7a}$$

$$T_3^{\mathrm{HF}}=\frac{\tilde{n}_1 i\tilde{q}_2}{4}+\frac{\tilde{n}_2(1+i\tilde{q}_1)}{2}-\frac{\tilde{n}_1^2(1+i\tilde{q}_1)}{4n_0}-\frac{(i\tilde{q}_1\tilde{n}_2+i\tilde{q}_2\tilde{n}_1)(3\tilde{\omega}^2+i\gamma\tilde{\omega})}{n_0}+\frac{3i\tilde{q}_1\tilde{n}_1^2(3\tilde{\omega}^2+i\gamma\tilde{\omega})}{4n_0^2}+\frac{\tilde{n}_1^3\tilde{f}_0}{4n_0^2}-\frac{3\tilde{n}_1\tilde{n}_2\tilde{f}_0}{n_0}+\frac{\tilde{n}_1 i\tilde{q}_2\tilde{f}_0'}{n_0}$$
$$+\frac{2\tilde{n}_2 i\tilde{q}_1\tilde{f}_0'}{n_0}+\frac{\tilde{n}_1^2 i\tilde{q}_1\tilde{f}_0'}{2n_0^2}-\frac{i\tilde{q}_1 i\tilde{q}_2\tilde{f}_0''}{2n_0}-\frac{(i\tilde{q}_1)^2\tilde{n}_1\tilde{f}_0''}{2n_0^2}+\frac{(i\tilde{q}_1)^3\tilde{f}_0'''}{12n_0^2}+\frac{\tilde{\omega}^2(i\tilde{q}_1)^2\{n_0+i\tilde{q}_1(n_0-\tilde{\omega}^2-i\gamma\tilde{\omega})\}}{12n_0^2}$$
$$+\frac{(i\tilde{q}_1)^2\tilde{n}_1\tilde{f}_0(2n_0-11\tilde{\omega}^2-4i\gamma\tilde{\omega})}{4n_0^2}+\frac{(i\tilde{q}_1\tilde{n}_1-i\tilde{q}_2n_0)\tilde{f}_0}{2n_0}+\frac{i\tilde{q}_1 i\tilde{q}_2\tilde{f}_0(7\tilde{\omega}^2+3i\gamma\tilde{\omega}-2n_0)}{2n_0}+\frac{3(i\tilde{q}_2\tilde{n}_1+2i\tilde{q}_1\tilde{n}_2)\tilde{f}_0^2}{2n_0}$$
$$+\frac{(i\tilde{q}_1)^2(1+i\tilde{q}_1)\tilde{f}_0'}{4n_0}+\frac{(i\tilde{q}_1)^3\tilde{f}_0'^2}{3n_0^2}-\frac{(i\tilde{q}_1)^3\tilde{f}_0'(5\tilde{\omega}^2+3i\gamma\tilde{\omega})}{12n_0^2}-\frac{9(i\tilde{q}_1)^2\tilde{n}_1\tilde{f}_0\tilde{f}_0'}{4n_0^2}-\frac{3i\tilde{q}_1 i\tilde{q}_2\tilde{f}_0\tilde{f}_0'}{2n_0}+\frac{(i\tilde{q}_1)^3\tilde{f}_0\tilde{f}_0''}{2n_0^2}+\frac{(i\tilde{q}_1)^3\tilde{f}_0^4}{2n_0^2}$$
$$+\frac{i\tilde{q}_1\tilde{f}_0^2\{-3i\tilde{q}_1n_0-3(i\tilde{q}_1)^2(n_0-3\tilde{\omega}^2-i\gamma\tilde{\omega})-18n_0i\tilde{q}_2\tilde{f}_0-9i\tilde{q}_1\tilde{n}_1\tilde{f}_0+20(i\tilde{q}_1)^2\tilde{f}_0'\}}{12n_0^2}. \tag{A7b}$$

*fomichev@imp.kiae.ru
†zaretsky@imp.kiae.ru
‡wbecker@mbi-berlin.de

[1] M. Lippitz, M. A. van Dijk, and M. Orrit, Nano Lett. **5**, 799 (2005).
[2] M. A. van Dijk, M. Lippitz, and M. Orrit, Acc. Chem. Res. **38**, 594 (2005).
[3] T.-M. Liu, S.-P. Tai, C.-H. Yu, Y.-C. Wen, S.-W. Chu, L.-J. Chen, M. R. Prasad, K.-J. Lin, and C.-K. Sun, Appl. Phys. Lett. **89**, 043122 (2006).
[4] B. Shim, G. Hays, R. Zgadzaj, T. Ditmire, and M. C. Downer, Phys. Rev. Lett. **98**, 123902 (2007).
[5] S. V. Fomichev, S. V. Popruzhenko, and D. F. Zaretsky, Laser Phys. **13**, 1188 (2003).
[6] S. V. Fomichev, S. V. Popruzhenko, D. F. Zaretsky, and W. Becker, J. Phys. B **36**, 3817 (2003).
[7] S. V. Fomichev, S. V. Popruzhenko, D. F. Zaretsky, and W. Becker, Opt. Express **11**, 2433 (2003).
[8] S. V. Fomichev, D. F. Zaretsky, and W. Becker, J. Phys. B **37**, L175 (2004).
[9] S. V. Fomichev, D. F. Zaretsky, D. Bauer, and W. Becker, Phys. Rev. A **71**, 013201 (2005).
[10] M. V. Fomyts'kyi, B. N. Breizman, A. V. Arefiev, and C. Chiu, Phys. Plasmas **11**, 3349 (2004).
[11] P. K. Tiwari and V. K. Tripathi, Phys. Scr. **74**, 682 (2006).
[12] U. Kreibig and M. Vollmer, *Optical Properties of Metal Clusters* (Springer-Verlag, Berlin, 1995).
[13] J.-H. Klein-Wiele, P. Simon, and H.-G. Rubahn, Phys. Rev. Lett. **80**, 45 (1998).
[14] S. V. Fomichev and D. F. Zaretsky, J. Phys. B **32**, 5083 (1999).
[15] P. Mulser, M. Kanapathipillai, and D. H. H. Hoffmann, Phys. Rev. Lett. **95**, 103401 (2005).
[16] P. Mulser and M. Kanapathipillai, Phys. Rev. A **71**, 063201 (2005).
[17] Ph. A. Korneev, S. V. Popruzhenko, D. F. Zaretsky, and W. Becker, Laser Phys. Lett. **2**, 452 (2005).
[18] M. Kundu and D. Bauer, Phys. Rev. Lett. **96**, 123401 (2006).
[19] M. Kundu and D. Bauer, Phys. Rev. A **74**, 063202 (2006).
[20] V. G. Babaev, R. V. Volkov, V. M. Gordienko, M. S. Dzhidzhoev, M. A. Zhukov, V. V. Kolchin, A. B. Savel'ev, A. P. Tarasevitch, and A. A. Shashkov, Quantum Electron. **27**, 283 (1997).
[21] F. Greschik, L. Dimou, and H. J. Kull, Laser Part. Beams **18**, 367 (2000).
[22] A. V. Andreev and A. B. Kozlov, Phys. Rev. B **68**, 195405 (2003).
[23] D. F. Zaretsky, Ph. A. Korneev, S. V. Popruzhenko, and W. Becker, J. Phys. B **37**, 4817 (2004).
[24] A. J. McAlister and E. A. Stern, Phys. Rev. **132**, 1599 (1963).
[25] N. Takimoto, Phys. Rev. **154**, 369 (1967).
[26] A. R. Melnyk and M. J. Harrison, Phys. Rev. B **2**, 835 (1970).
[27] L. G. Gerchikov, C. Guet, and A. N. Ipatov, Phys. Rev. A **66**, 053202 (2002).
[28] A. R. Holkundkar and N. K. Gupta, Phys. Plasmas **15**, 013105 (2008).
[29] F. Calvayrac, P.-G. Reinhard, E. Suraud, and C. A. Ullrich, Phys. Rep. **337**, 493 (2000).
[30] P.-G. Reinhard and E. Suraud, *Introduction to Cluster Dynamics* (Wiley, Berlin, 2003).
[31] G. Manfredi and P. A. Hervieux, Phys. Rev. B **70**, 201402(R) (2004).
[32] G. Manfredi and P. A. Hervieux, Opt. Lett. **30**, 3090 (2005).
[33] G. Manfredi and P. A. Hervieux, Phys. Rev. B **72**, 155421 (2005).
[34] J. E. Sipe, V. C. Y. So, M. Fukui, and G. I. Stegeman, Phys. Rev. B **21**, 4389 (1980).
[35] M. Corvi and W. L. Schaich, Phys. Rev. B **33**, 3688 (1986).
[36] W. L. Schaich and A. Liebsch, Phys. Rev. B **37**, 6187 (1988).
[37] J. A. Maytorena, W. L. Mochan, and B. S. Mendoza, Phys. Rev. B **51**, 2556 (1995).
[38] C. Kittel, *Introduction to Solid State Physics*, 5th ed. (Wiley, New York, 1976).
[39] V. P. Silin, *Vvedenie v Kineticheskuyu Teoriyu Gazov* (Nauka, Moscow, 1971).
[40] E. M. Lifshitz and L. P. Pitaevsky, *Course of Theoretical Physics: Physical Kinetics* (Pergamon, Oxford, 1981), Vol. X.
[41] L. D. Landau and E. M. Lifshitz, *Course of Theoretical Physics: Statistical Physics, Part 1*, 3rd ed., (Pergamon, Oxford, 1980), Vol. V.
[42] A. Bergmann, S. Hüller, P. Mulser, and H. Schnabl, Europhys. Lett. **14**, 661 (1991).
[43] A. Bergmann and P. Mulser, Phys. Rev. E **47**, 3585 (1993).
[44] W. B. Mori and T. Katsouleas, Phys. Scr. **T30**, 127 (1990).
[45] P. Gibbon, *Short Pulse Laser Interactions with Matter* (Imperial College Press, London, 2005).
[46] Lu Hu and Gang Chen, Nano Lett. **7**, 3249 (2007).